[4], and Zweier et al. found a single *TBX1* mutation after examining 10 patients with 22q11.2DS phenotype [8]. This indicates the presence of genetic heterogeneity in the development of 22q11.2DS phenotype in deletion-negative patients. Consistent with this, another DGS/VCFS locus has been assigned to chromosome 10p13-14 region [9]. Thus, it would be reasonable to perform a comprehensive genetic analysis in deletion-negative patients with 22q11.2DS phenotype.

In this regard, recent advance in molecular technologies has enabled to perform comprehensive genetic analyses, thereby contributing to the identification of underlying factors in genetic disorders. Indeed, genomewide array comparative genomic hybridization (CGH) has identified multiple disease-associated copy-number changes [10], and exome sequencing has discovered multiple disease-causing gene mutations [11]. In particular, these technologies can be powerful methods for familial disorders, because it is predicted that a single copy-number change or mutation is shared in common by affected subjects and is absent from non-affected subjects within a family.

Here, we performed array CGH analysis and exome sequencing in a family with 22q11.2DS-like clinical features. Although this study did not discover a novel disease gene, a *TBX1* mutation was successfully identified.

Materials and Methods

Ethics statement

The Institutional Review Board Committees of Hamamatsu University School of Medicine, Tohoku University School of Medicine, Kurashiki Central Hospital, and National Research Institute for Child Health and Development considered and approved the study, consent/assent procedures, and the publication of images and case details associated with this work. The individuals in this manuscript have given written informed consent (as outlined in PLOS consent form) to publish these case details. Actually, this study was performed after obtaining written informed consent from the parents of the child subjects and from the adult subjects. Furthermore, the mother and the elder brother aged 19 years old have given written informed consent to publication of the facial photographs of the two brothers; in addition, the younger brother aged 10 years has given informed assent.

Clinical Report

The pedigree of this Japanese family is shown in Fig. 1, and clinical findings of the family members are summarized in Table 1. The proband (subject III-5) was found to have hypocalcemia and hyperphosphatemia in a pre-operation laboratory test for repeated otitis media at 8 years of age, and was referred to Department of Pediatrics at Kurashiki Central Hospital. Subsequent examination revealed borderline low serum intact PTH value. Thus, he was diagnosed as having hypoparathyroidism, and received vitamin D therapy. Furthermore, physical examination showed characteristic craniofacial features with velopharyngeal incompetence suggestive of 22q11.2DS.

Similar craniofacial features were also exhibited by subjects II-2, III-1, III-6, and III-7, and hypocalcemia was also identified in subjects II-2 and III-7. Actually, subject II-2 was taking vitamin D, and subject III-7 was noticed to have hypocalcemia at birth because of the history of subject III-5, and was treated with vitamin D. The five subjects with 22q11.2DS-like craniofacial features lacked cardiovascular anomalies; while they also lacked susceptibility to infection, except for repeated otitis media in subject III-5, thymic hypoplasia was not evaluated in four of the five subjects. By contrast, the five subjects exhibited borderline to mild developmental delay. Indeed, adult subjects II-2 and III-1 had some difficulty in verbal communications, although they were able to get on their daily life, and subject II-2 was able to take care of family members. Similarly, child subjects III-5, III-6, and III-7 also showed speech delay, and subjects III-5 and III-7 received speech therapy. Furthermore, subject III-7 was diagnosed as having pervasive developmental disorder, and his verbal, performance, and full scale intelligence quotients were assessed as 63, 64, and 60, respectively, by the WISC-III method at 10 years of age. In addition, subject II-2 had sensorineural deafness, and subject III-5 had Graves' disease.

Molecularly Studied Subjects

Molecular studies were performed for eight subjects in this family, using peripheral blood samples. They were divided into three groups in terms of clinical findings: group 1, subjects II-2, III-5, and III-7 with craniofacial features and hypocalcemia; group 2, subjects III-1 and III-6 with craniofacial features alone; and group 3, subjects II-1, III-3, and IV-1 with apparently normal phenotype (Fig. 1).

FISH and Array CGH Analyses

Fluorescence *in situ* hybridization (FISH) analysis was performed with a probe for *HIRA* on the commonly deleted chromosome 22q11.2 region and that for *ARSA* at chromosome 22q13 utilized as an internal control (Abott). Array CGH was carried out using a genomewide 2x400K Agilent platform catalog array, according to the manufacturer's instructions (Agilent Technologies), and copy number variants/polymorphisms were screened with Agilent Genomic Workbench software using the Database of Genomic Variants (http://dgv.tcag.ca/dgv/app/home).

Exome and Sanger Sequencings

Exon capture was performed with the SureSelect Human All Exon kit v4 (Agilent Technologies). Exon libraries were sequenced with the Illumina Hiseq 2000 platform according to the manufacturer's instructions (Illumina), providing 108–122 average depth for each sample. Paired 101-base pair reads were aligned to the reference human genome (UCSChg19) using the Burrows-Wheeler Alignment tool [12]. Likely PCR duplicates were removed with the Picard program (http://picard.sourceforge.net/). Single-nucleotide variants and indels were identified using the Genome Analysis Tool Kit (GATK) v1.6 software [13]. SNVs and indels were annotated against the RefSeq database, 1000 Genomes Project variant data, and dbSNP135 with the ANNOVAR program [14].

To confirm mutations indicated by exome sequencing, Sanger sequencing was performed for PCR products obtained with primers flanking the detected mutations, using a 3500xL genetic analyzer (Life Technologies). Furthermore, the PCR products were subcloned with TOPO TA Cloning Kit (Life Technologies), and normal and mutant alleles were sequenced separately.

In silico protein functional analysis

Function of proteins with missense variations was assessed by Polymorphism Phenotyping-2 (PolyPhen-2, http://genetics.bwh.harvard.edu/pph2/) and Sorting Intolerant From Tolerant (SIFT, http://sift.jcvi.org/), and that of proteins with in-frame amino acid deletions was evaluated by PROVEAN predictions (http://provean.jcvi.org/index.php).

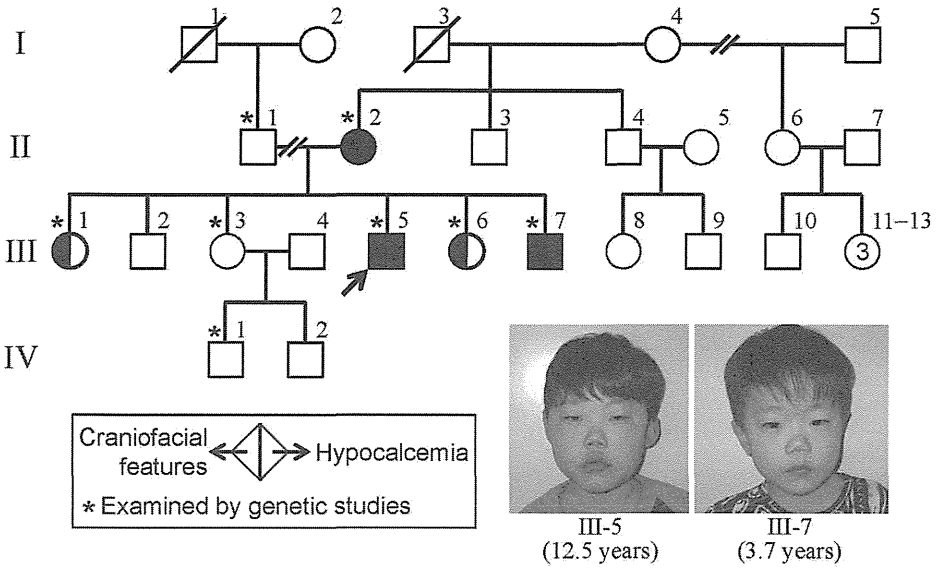

Figure 1. The pedigree of this family. Facial features of subjects III-5 and III-7 are shown.
doi:10.1371/journal.pone.0091598.g001

Results

FISH and Array CGH Analyses

FISH analysis delineated two signals for *HIRA* (Fig. 2A). Array CGH analysis revealed no copy number change specific to group 1 or groups 1+2, in the entire genome including chromosome 10p13-14 and chromosome 22q11.2 regions (Fig. 2B).

Exome and Sanger Sequencings

Exome sequencing identified nine heterozygous non-synonymous variants (six missense variants, two in-frame microdeletions, and one frameshift variant) that were specific to groups 1+2 (namely, they were present in groups 1+2 and absent from group 3 as well as from 1000 Genomes, dbSNP135, and our in-house exome data from 70 individuals) (Table S1). Notably, the frameshift variant (c.1253delA, p.Y418fsX459) was found at exon 9C of *TBX1* for DGS/VCFS (Fig. 3). Of the remaining eight variants, two variants were also detected in disease-related genes: p.G204R in *HDAC4* for brachydactyly-mental retardation syndrome [15], and p.276del in *CCND1* constituting a susceptibility factor for colorectal cancer and a modifier for von Hippel-Lindau disease [16,17]. Exome sequencing also detected two heterozygous missense variants that were specific to group 1 (Table S1).

When all variants were included, exome sequencing revealed: (1) 83 non-synonymous and 86 synonymous variants that were present in groups 1+2 and absent from group 3 (Table S2); (2) 54 non-synonymous and 48 synonymous variants that were present in group 1 and absent from groups 2+3 (Table S3); (3) 6,033 non-synonymous and 6,667 synonymous variants that were present in groups 1+2, but not specific to groups 1+2 (thus, they may be present in group 3 or absent from group 3); and (4) 7,073 non-synonymous and 7,861 synonymous variants that were present in group 1, but not specific to group 1. Furthermore, comparison of the exome sequencing data between group 1 with hypocalcemia and group 2 without hypocalcemia revealed 231 non-synonymous and 254 synonymous variants that were present in group 1 and absent from group 2 (Table S4), and 246 non-synonymous and 242 synonymous variants that were present in group 2 and absent from group 1 (Table S5). (The variant data other than those described in Supplemental Tables may be available on request after discussion with the family members and approval by our IRBs, because they contain a huge amount of individual genetic information.)

In silico protein functional analysis

The results are summarized in Table S1. The p.G204R in *HDAC4* and the p.E276del in *CCND1* were assessed as non-pathologic, while some variants were evaluated as potentially pathologic.

Discussion

Exome sequencing successfully identified a heterozygous frameshift variant on exon 9C of *TBX1*. The c.1253delA (p.Y418fsX459) appears to be a disease-causing mutation, because it is predicted that this variant escapes nonsense-mediated mRNA decay due to its position on the final exon [18] and produces a truncated protein lacking the nuclear localization signal (NLS) and most of the transactivation domain (TAD) on exon 9C (Fig. 3) [19]. In support of this, functional studies for a similar c.1223delC (p.S408fsX459) mutation on exon 9C have shown that the truncated p.S408fsX459 protein was incapable of localizing to nucleus and lost transactivation function [2,5,19]. One may argue that this c.1253delA mutation affects *TBX1* isoform C (*TBX1C*, TBX1-003) alone, while *TBX1* produces three transcript variants containing T-box [2,4] (Fig. 3). However, *TBX1C* is the major transcript with the NLS and the TAD in human and is highly homologous to mouse *Tbx1* [4] (Fig. S1).

Craniofacial features in groups 1+2 and hypocalcemia in group 1 are well explained by the *TBX1* mutation [3]. This argues for a critical role of this mutation in the phenotypic development in groups 1+2, while the clinical effects of the remaining variants identified by exome sequencing are largely unknown. In this regard, comparison between group 1 with hypocalcemia and group 2 without hypocalcemia revealed a large number of non-synonymous and synonymous variants that exclusively belonged to either group 1 (Table S4) or group 2 (Table S5), although the lists did not contain a c.2968A>G (p.R990G) SNP in *CASR* (calcium sensing receptor) that has a gain-of-function effect and appears to raise the susceptibility to hypocalcemia (Fig. S2) [20]. Thus, it is

Table 1. Clinical findings of the family members.

	TBX1 mutation (+)					*TBX1* mutation (−)			*TBX1* mutation (N.E.)		
Individual	**II-2**	**III-1**	**III-5**	**III-6**	**III-7**	**II-1**	**III-3**	**IV-1**	**II-3**	**II-4**	**III-2**
Present age (year)	51	26	19	13	10	59	22	5	50	49	25
Sex	F	F	M	F	M	M	F	M	M	M	M
Craniofacial features	+	+	+	+	+	−	−	−	−	−	−
Hypertelorism	+	+	+	+	+	−	−	−	−	−	−
Blepharophimosis	+	+	+	+	+	−	−	−	−	−	−
Low set ears	+	+	+	+	+	−	−	−	−	−	−
Auricular anomalies	+	−	−	−	−	−	−	−	−	−	−
Narrow nose	+	+	+	+	+	−	−	−	−	−	−
Cleft palate	−	−	−	−	−	−	−	−	−	−	−
Micrognathia	±	+	+	+	+	−	−	−	−	−	−
Velopharyngeal incompetence	+[d]	+	+	+	+	−	−	−	−	−	−
Hypoparathyroidism	+	−	+	−	+	−	−	−	−	−	−
Age at examination (year)	44	17	8	4	0 (1 day)	N.E.	15	0 (6 days)	N.E.	N.E.	18
Serum calcium (mg/dL)[a]	7.6[e]	9.0	6.0	9.1	5.9	...	9.0	9.8	...	...	9.6
Serum i-phosphate (mg/dL)[a]	3.9[e]	4.9	9.1	5.0	N.E.	...	4.8	6.3	...	...	4.6
Serum intact PTH (pg/dL)[a]	31[e]	N.E.	15	N.E.	19	...	N.E.	34	...	...	N.E.
Cardiovascular anomalies[b]	−	−	−	−	−	−	−	−	−	−	−
Hypoplastic thymus[c]	−	N.E.	N.E.	N.E.	N.E.	N.E.	N.E.	N.E.	N.E.	N.E.	N.E.
Susceptible to infection	−	−	−[f]	−	−	−	−	−	−	−	−
Other features	−	−	−	−	−	−	−	−	−	−	−
Developmental retardation	+	+	+[g]	+	+[g]	−	−	−	−	−	−
Sensorineural deafness	+[h]	−	−	−	−	−	−	−	−	−	−
Graves' disease	−	−	+[i]	−	−	−	−	−	−	−	−

Individuals correspond to those shown in Fig. 1.
i-phosphate: inorganic phosphate; SD: standard deviation; F: female; M: male; and N.E.: not examined.
[a]Reference values: calcium, 9.0–11.0 mg/dL in infants and 8.8–10.2 mg/dL in adults; inorganic phosphate, 4.8–7.5 mg/dL in infants and 2.5–4.5 mg/dL in adults, and intact PTH, 10–65 pg/dL in infants and 14–55 pg/dL in adults.
Conversion factor to the SI unit: 0.25 for calcium (mmol/L), 0.32 for inorganic phosphate (mmol/L), and 0.106 for intact PTH (pmol/L).
[b]Examined by echocardiography, chest roentgenography, and/or electrocardiography.
[c]Examined by computed tomography.
[d]Received velopharyngeal closure.
[e]On treatment with vitamin D.
[f]Repeated otitis media only.
[g]Received speech therapy.
[h]Required hearing aids.
[i]At the time of diagnosis (11 years of age), serum TSH was <0.01 mIU/L, free T_3 33.1 pg/mL [51.0 pmol/L], free T_4 5.11 ng/dL [65.8 nmol/L], and TSH receptor antibody 1284% [normal range <1.9%].
doi:10.1371/journal.pone.0091598.t001

likely that, together with environmental factors, the combination of hitherto unknown calcium metabolism-related functional variants would underlie different serum calcium values between groups 1 and 2.

In addition to craniofacial features with and without hypocalcemia, *TBX1* mutation positive subject II-2 had sensorineural deafness, and III-5 had Graves' disease. Since such features are occasionally manifested by patients with 22q11.2DS [21,22], the results may suggest the relevance of *TBX1* to such rather infrequent features in 22q11.2DS.

The five *TBX1* mutation positive subjects in groups 1+2 lacked cardiovascular lesion and manifested borderline to mild developmental retardation (while they had no susceptibility to infection, assessment of thymic hypoplasia remained fragmentary). By contrast, cardiovascular lesion is frequently observed and developmental retardation is rare in previously reported patients with *TBX1* mutations, although clinical features are fairly variable among mutation positive patients (Table 2). Such difference would more or less be ascribed to an examination bias that *TBX1* has been analyzed in patients with isolated cardiovascular lesion in several studies [4,6,7] or to the functional difference of the mutant proteins [2,5–8]. However, in seven patients who have been examined for DGS/VCFS-like clinical features and found to have frameshift mutations on exon 9C (p.S408fsX459, p.H425fsX613, and p.S431fsX608) affecting the NLS and the TAD, cardiovascular lesion was present in four patients and developmental delay was absent or not described, despite apparent similarity in the ascertainment of patients and the function of mutant proteins between the seven patients and the five affected subjects in this family (Table 2) [2–5].

Thus, there may be protective factor(s) for cardiovascular lesion and susceptibility factor(s) for developmental delay in groups 1+2.

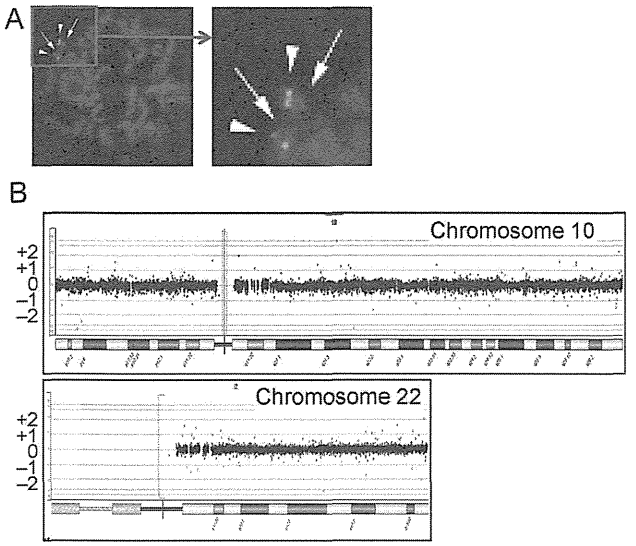

Figure 2. FISH and array CGH analyses in the proband (III-5). A. FISH analysis. Two signals are shown for both *HIRA* at 22q11.2 (red signals indicated by arrows) and *ARSA* at 22q13 (green signals indicated by arrowheads). **B.** Array CGH analysis. No copy number change is found for chromosome 10 carrying the second DiGeorge region and chromosome 22 harboring the DGS/VCFS critical region, as well as other chromosomes (not shown). Black, red, and green dots denote signals indicative of the normal, the increased (>+0.5), and the decreased (<−0.8) copy numbers, respectively. Although several red and green signals are seen, there is no portion associated with ≥3 consecutive red or green signals.
doi:10.1371/journal.pone.0091598.g002

In this regard, a simple explanation would be that protective factor(s) for cardiovascular lesion are present in groups 1+2 and may be present in group 3 or absent from group 3, whereas susceptibility factor(s) for developmental delay is present in groups 1+2 and absent from group 3. Since 6,033 non-synonymous and 6,667 synonymous variants were found to be present in groups 1+2 but not specific to groups 1+2, and 83 non-synonymous and 86 synonymous variants were revealed to be present in groups 1+2 and absent from group 3, a certain fraction of functional variants may constitute protective factor(s) for cardiovascular lesion and susceptibility factor(s) for developmental delay. In addition, while p.G204R on *HDAC4* for brachydactyly-mental retardation syndrome was assessed as non-pathologic by *in silico* analysis, it may have played a certain role in the occurrence of developmental delay in groups 1+2. Actually, such protective and susceptibility factor(s) would be more complex, with the effects of functional variants unique to each patient as well as the influences of environmental factors. Furthermore, it remains possible that the c.1253delA (p.Y418fsX459) mutation found in this study may be related to a specific phenotype characterized by the presence of craniofacial features and developmental delay and by the absence of cardiovascular lesion, because of a hitherto unrevealed mechanism(s). This matter awaits further studies.

Besides the clinical findings, several matters are also notable in the nine apparently pathologic *TBX1* mutations identified to date (Table 2). First, the mutations reside on exons 3–8 common to isoforms A–C or on exon 9C specific to isoform C, with no mutation on exons 9A and 9B specific to isoforms A and B. This would be consistent with *TBX1C* having the primary biological function. Second, while most mutations have loss-of-function effects, gain-of-function effects have been suggested for p.F148Y, p.H194Q, and p.310S by *in vitro* studies [8]. Thus, *TBX1* loss-of-function mutations and gain-of-function mutations may result in overlapping clinical features. Lastly, the c.1274_1281delACTATCTC (p.H425fsX613) missing the NLS on exon 9C was shared by a patient with DGS-like phenotype and the apparently normal mother, and the c.129_185del57 (p.43-61del19) with reduced transcriptional activity was common to a patient with non-syndromic tetralogy of Fallot and the apparently normal mother. This would imply the reduced penetrance of phenotypes caused by these mutations.

In summary, we identified a *TBX1* mutation by exome sequencing in a family with chromosome 22q11.2 deletion-like

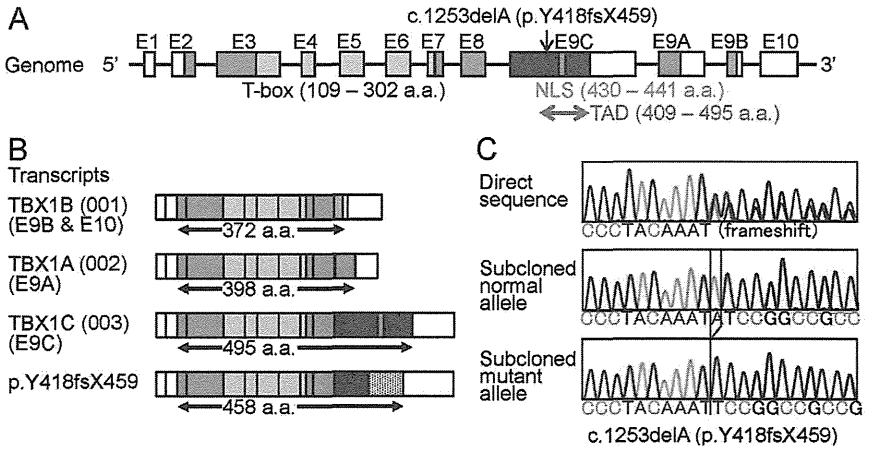

Figure 3. *TBX1* mutation identified in this family. A. Genomic structure of *TBX1* and the position of the mutation. The color and the white boxes represent the coding regions and the untranslated regions on exons 1–10 (E1–E10), respectively; the red, the purple, and the orange segments indicate the coding regions on the final exons 9C, 9A, and 9B (splice variants), respectively. The T-box is indicated by yellow boxes, the nuclear localization signal (NLA) by a blue segment, and the transactivation domain (TAD) by a green arrow. The c.1253delA (p.Y418fsX459) identified in this family resides on exon 9C. **B.** Transcripts of *TBX1*. Three variants are formed by alternative splicing of the final exons 9C, 9A, and 9B. The c.1253delA (p.Y418fsX459) mutation is predicted to yield a truncated TBX1C protein missing the NLS and most of the TAD. The stippled box of p.Y418fsX459 denotes aberrant amino acid sequence produced by the frameshift mutation. **C.** Electrochromatograms showing the frameshift mutation by Sanger sequencing. The primer sequences used are: 5′-GCGGCCAAGAGCCTTCTCT-3′ and 5′-GGGTGGTAGCCGTGGCCA-3′.
doi:10.1371/journal.pone.0091598.g003

Table 2. Summary of patients with *TBX1* mutations.

	TBX1C only					TBX1A–C				22q11.2DS
Position	**Exon 9C**	**Exon 9C**	**Exon 9C**	**Exon 9C**	**Exon 9C**	**Exon 3**	**Exon 4**	**Exon 5**	**Exon 8**	
cDNA change[a]	c.1223	c.1253	c.1274_1281	c.1293_1315	c.1399_1428	c.129_185	c.443T>A	c.582C>G	c.928G>A	Deletion
	delC	delA	del8	del23[h]	dup30[k]	del57[k]				
Amino acid	p.S408	p.Y418	p.H425	p.S431	p.467_476	p.43_61	p.F148Y	p.H194Q	p.G310S	
change	fsX459	fsX459	fsX613	fsX608	dup10A	del19				
NLS (exon 9C)	–	–	–	+[i]	+[l]	+	+	+	+	
TAD (exon 9C)	–	Involved	Involved	Involved	Involved	+	+	+	+	
Function	LOF	N.E.	N.E.	LOF	LOF	Reduced	GOF[m]	GOF[m]	GOF[m]	
Patient number	3	5	1	3[j]	2	1	1	2	1	558
Occurrence	Familial	Familial	Sporadic[g]	Familial	Sporadic	Sporadic[g]	Sporadic	Familial	Sporadic	
Facial features[b]	3/3	5/5	+	3/3	0/2	–	+	2/2	+	100%
Nasal voice[c]	2/3	5/5	N.D.	3/3	0/2	–	+	0/2	+	32%
Cardiovascular anomalies	1/3	0/5	+	2/3	2/2	+	+	0/2	+	57%
Hypopara-thyroidism[d]	1/3	3/5	+	N.D.	0/2	–	–	0/2	+	60%
Hypoplastic thymus	1/2[e]	0/1[f]	+	N.D.	0/2	–	–	N.E.	+	?
Susceptible to infection	N.D.	0/5	N.D.	N.D.	0/2	–	N.D.	N.D.	N.D.	?
Developmental retardation	0/3	5/5	N.D	0/3	0/2	–	–	1/2	–	38%
Reference	2	This study	3, 4	5	4, 6	7	2	8	2	1

In addition to the mutations listed in this table, several missense variants and in-frame indels with unknown functions have been found in patients with isolated cardiovascular anomalies and in those with DGS/VCFS-like phenotype [4].
NLS: nuclear localization signal; TAD: transactivation domain; LOF: loss-of-function; N.D.: not described; N.E.: not examined; GOF: gain-of-function; Del: deletion; and Dup: duplication.
[a]According to NM_080647.
[b]Suggestive of 22q11.2 deletion syndrome.
[c]Velopharygeal insufficiency.
[d]Hypocalcemia is included.
[e]Two of the three subjects have been examined for hypoplastic thymus.
[f]One of the five subjects has been examined for hypoplastic thymus.
[g]These two mutations have been inherited from apparently normal mothers.
[h]The c.1293-1315del23 has been described as c.1320-1342del23 in the original report [5].
[i]Although the natural NLS has been disrupted, a new NLS-compatible motif (RGRRRRCR) has been created on the added amino acid sequence.
[j]Another deceased individual in this family also has similar clinical features.
[k]These two mutations have been identified in *TBX1* analyses for patients with cardiovascular anomalies only.
[l]The mutant protein is aggregated in the cytoplasm and the nucleus.
[m]Gain-of-function effects have been found by *in vitro* studies [8].
doi:10.1371/journal.pone.0091598.t002

phenotype. Application of such powerful methods will serve to identify a causative gene in genetically heterogeneous disorders.

Supporting Information

Figure S1 Comparison of amino acid sequence of human *TBX1C* and mouse *Tbx1*. The T-box is highlighted in yellow, and the nuclear localization signal in light blue. The region for transactivation domain is surrounded by squares. The Y highlighted in red denotes the amino acid residue where the frameshift mutation in this family has taken place.
(TIF)

Figure S2 Analysis of c.2968A>G SNP (p.R990G, rs1042636) with a gain-of-function effect in exon 7 of *CASR*. The SNP pattern is not co-segregated with the presence or absence of hypocalcemia.
(TIF)

Table S1 Summary of heterozygous non-synonymous variants.
(PDF)

Table S2 A list of variants that are present in groups 1+2 and absent from group 3.
(PDF)

Table S3 A list of variants that are present in group 1 and absent from groups 2+3.
(PDF)

Table S4 A list of variants that are present in group 1 and absent from group 2.
(PDF)

Table S5 A list of variants that are present in group 2 and absent from group 1.
(PDF)

References

1. Ryan AK, Goodship JA, Wilson DI, Philip N, Levy A, et al. (1997) Spectrum of clinical features associated with interstitial chromosome 22q11 deletions: a European collaborative study. J Med Genet 34: 798–804.
2. Yagi H, Furutani Y, Hamada H, Sasaki T, Asakawa S, et al. (2003) Role of TBX1 in human del22q11.2 syndrome. Lancet 362: 1366–1373.
3. Baldini A (2005) Dissecting contiguous gene defects: TBX1. Curr Opin Genet Dev 15: 279–84.
4. Gong W, Gottlieb S, Collins J, Blescia A, Dietz H, et al. (2001) Mutation analysis of TBX1 in non-deleted patients with features of DGS/VCFS or isolated cardiovascular defects. J Med Genet 38: E45.
5. Paylor R, Glaser B, Mupo A, Ataliotis P, Spencer C, et al. (2006) Tbx1 haploinsufficiency is linked to behavioral disorders in mice and humans: implications for 22q11 deletion syndrome. Proc Natl Acad Sci U S A 103: 7729–7734.
6. Rauch R, Hofbeck M, Zweier C, Koch A, Zink S, et al. (2010) Comprehensive genotype-phenotype analysis in 230 patients with tetralogy of Fallot. J Med Genet 47: 321–331.
7. Griffin HR, Töpf A, Glen E, Zweier C, Stuart AG, et al. (2010) Systematic survey of variants in TBX1 in non-syndromic tetralogy of Fallot identifies a novel 57 base pair deletion that reduces transcriptional activity but finds no evidence for association with common variants. Heart 96: 1651–1655.
8. Zweier C, Sticht H, Aydin-Yaylagül I, Campbell CE, Rauch A (2007) Human TBX1 missense mutations cause gain of function resulting in the same phenotype as 22q11.2 deletions. Am J Hum Genet 80: 510–517.
9. Daw SCM, Taylor C, Kraman M, Call K, Mao J, et al. (1996) A common region of 10p deleted in DiGeorge and velocardiofacial syndromes. Nat Genet 13: 458–461.
10. McDonnell SK, Riska SM, Klee EW, Thorland EC, Kay NE, et al. (2013) Experimental designs for array comparative genomic hybridization technology. Cytogenet Genome Res 139: 250–257.
11. Wang Z, Liu X, Yang B-Z, Gelernter J (2013) The role and challenges of exome sequencing in studies of human diseases Front Genet doi: 10.3389/fgene.2013.00160.
12. Li H, Durbin R (2009) Fast and accurate short read alignment with Burrows-Wheeler transform. Bioinformatics 25: 1754–1760.
13. McKenna A, Hanna M, Banks E, Sivachenko A, Cibulskis K, et al. (2010) The Genome Analysis Toolkit: a MapReduce framework for analyzing next-generation DNA sequencing data. Genome Res 20: 1297–1303.
14. Wang K, Li M, Hakonarson H (2010) ANNOVAR: functional annotation of genetic variants from high-throughput sequencing data. Nucleic Acids Res 38: e164.
15. Williams SR, Aldred MA, Der Kaloustian VM, Halal F, Gowans G, et al (2010). Haploinsufficiency of HDAC4 causes brachydactyly mental retardation syndrome, with brachydactyly type E, developmental delays, and behavioral problems. Am J Hum Genet 87: 219–228.
16. Kong S, Amos CI, Luthra R, Lynch PM, Levin B, et al. (2000) Effects of cyclin D1 polymorphism on age of onset of hereditary nonpolyposis colorectal cancer. Cancer Res 60: 249–252.
17. Zatyka M, da Silva NF, Clifford SC, Morris MR, Wiesener MS, et al (2002). Identification of cyclin D1 and other novel targets for the von Hippel-Lindau tumor suppressor gene by expression array analysis and investigation of cyclin D1 genotype as a modifier in von Hippel-Lindau disease. Cancer Res 62: 3803–3811.
18. Holbrook JA, Neu-Yilik G, Hentze MW, Kulozik AE (2004) Nonsense-mediated decay approaches the clinic. Nat Genet 36: 801–808.
19. Stoller JZ, Epstein JA (2005) Identification of a novel nuclear localization signal in Tbx1 that is deleted in DiGeorge syndrome patients harboring the 1223delC mutation. Hum Mol Genet 14: 885–892.
20. Vezzoli G, Terranegra A, Arcidiacono T, Biasion R, Coviello D, et al. (2007) R990G polymorphism of calcium-sensing receptor does produce a gain-of-function and predispose to primary hypercalciuria. Kidney Int 71: 1155–1162.
21. Ohtani I, Schuknecht HF (1984) Temporal bone pathology in DiGeorge's syndrome. Ann Otol Rhinol Laryngol 93(3 Pt 1): 220–224.
22. Kawame H, Adachi M, Tachibana K, Kurosawa K, Ito F, et al. (2001) Graves' disease in patients with 22q11.2 deletion. J Pediatr 139: 892–895.

Author Contributions

Conceived and designed the experiments: TO YM. Performed the experiments: T. Niihori SN FK MF YA. Analyzed the data: T. Nagashima RF KN. Contributed reagents/materials/analysis tools: KN. Wrote the manuscript: TO. Collected the clinical findings: NT MK.

Gain-of-Function Mutations in *RIT1* Cause Noonan Syndrome, a RAS/MAPK Pathway Syndrome

Yoko Aoki,[1,*] Tetsuya Niihori,[1] Toshihiro Banjo,[2] Nobuhiko Okamoto,[3] Seiji Mizuno,[4] Kenji Kurosawa,[5] Tsutomu Ogata,[6] Fumio Takada,[7] Michihiro Yano,[8] Toru Ando,[9] Tadataka Hoshika,[10] Christopher Barnett,[11,12] Hirofumi Ohashi,[13] Hiroshi Kawame,[14] Tomonobu Hasegawa,[15] Takahiro Okutani,[16] Tatsuo Nagashima,[17] Satoshi Hasegawa,[18] Ryo Funayama,[19] Takeshi Nagashima,[19] Keiko Nakayama,[19] Shin-ichi Inoue,[1] Yusuke Watanabe,[2] Toshihiko Ogura,[2] and Yoichi Matsubara[1,20]

RAS GTPases mediate a wide variety of cellular functions, including cell proliferation, survival, and differentiation. Recent studies have revealed that germline mutations and mosaicism for classical RAS mutations, including those in *HRAS*, *KRAS*, and *NRAS*, cause a wide spectrum of genetic disorders. These include Noonan syndrome and related disorders (RAS/mitogen-activated protein kinase [RAS/MAPK] pathway syndromes, or RASopathies), nevus sebaceous, and Schimmelpenning syndrome. In the present study, we identified a total of nine missense, nonsynonymous mutations in *RIT1*, encoding a member of the RAS subfamily, in 17 of 180 individuals (9%) with Noonan syndrome or a related condition but with no detectable mutations in known Noonan-related genes. Clinical manifestations in the *RIT1*-mutation-positive individuals are consistent with those of Noonan syndrome, which is characterized by distinctive facial features, short stature, and congenital heart defects. Seventy percent of mutation-positive individuals presented with hypertrophic cardiomyopathy; this frequency is high relative to the overall 20% incidence in individuals with Noonan syndrome. Luciferase assays in NIH 3T3 cells showed that five RIT1 alterations identified in children with Noonan syndrome enhanced ELK1 transactivation. The introduction of mRNAs of mutant *RIT1* into 1-cell-stage zebrafish embryos was found to result in a significant increase of embryos with craniofacial abnormalities, incomplete looping, a hypoplastic chamber in the heart, and an elongated yolk sac. These results demonstrate that gain-of-function mutations in *RIT1* cause Noonan syndrome and show a similar biological effect to mutations in other RASopathy-related genes.

RAS GTPases are monomeric G proteins with a molecular mass of 20–40 kDa and cycle between a GTP-bound active and a GDP-bound inactive state. The members of the RAS superfamily are structurally classified into at least five subfamilies: RAS, Rho, Rab, Sar1/Arf, and Ran families.[1,2] The Ras subfamily consists of classical RAS proteins (HRAS, KRAS, and NRAS), RRAS, RRAS2 (TC21), RRAS3 (MRAS), RAPs, RAEB, RALs, RIT1, and RIT2 (RIN). RAS proteins interact with multiple effectors, including RAF kinases, phosphatidylinositol 3-kinase (PI-3 kinase), RalGDS, p120GAP, MEKK1, RIN1, AF-6, phospholipase C epsilon, and the Nore-MST1 complex, and activate multiple downstream signaling cascades.[1,2] Of these signaling pathways, the RAS/mitogen-activated protein kinase (RAS/MAPK) signaling pathway plays a central role in cellular proliferation and differentiation.

Noonan syndrome (MIM 163950) is an autosomal-dominant disorder characterized by short stature, distinctive facial features, and congenital heart defects.[3,4] The distinctive facial features include hypertelorism, downslanting palpebral fissures, ptosis, a webbed or short neck, and low-set, posteriorly rotated ears. Congenital heart defects, including pulmonary valve stenosis and atrial septal defects, occur in 50%–80% of individuals. Hypertrophic cardiomyopathy is observed in 20% of affected individuals. Other clinical manifestations include cryptorchidism, mild intellectual disability, bleeding tendency, and hydrops fetalis. The incidence of this syndrome is estimated to be between 1 in 1,000 to 1 in 2,500 live births. Individuals with Noonan syndrome are at risk of juvenile myelomonocytic leukemia (JMML), a myeloproliferative disorder characterized by excessive production of myelomonocytic cells.[4] Noonan syndrome exhibits phenotypic overlap

[1]Department of Medical Genetics, Tohoku University School of Medicine, Sendai 980-8574, Japan; [2]Department of Developmental Neurobiology, Institute of Development, Aging, and Cancer, Tohoku University, Sendai 980-8575, Japan; [3]Department of Medical Genetics, Osaka Medical Center and Research Institute for Maternal and Child Health, Izumi 594-1101, Japan; [4]Department of Pediatrics, Central Hospital, Aichi Human Service Center, Kasugai 480-0392, Japan; [5]Division of Medical Genetics, Kanagawa Children's Medical Center, Yokohama 232-8555, Japan; [6]Department of Pediatrics, Hamamatsu University School of Medicine, Hamamatsu 431-3192, Japan; [7]Department of Medical Genetics, Kitasato University Graduate School of Medical Sciences, Sagamihara 252-0373, Japan; [8]Department of Pediatrics, Akita University School of Medicine, Akita 010-8543, Japan; [9]Department of Pediatrics, Municipal Tsuruga Hospital, Tsuruga 914-8502, Japan; [10]Department of Pediatrics, Tottori Prefectural Central Hospital, Tottori 680-0901, Japan; [11]South Australian Clinical Genetics Service, SA Pathology, Women's and Children's Hospital, North Adelaide, Adelaide, SA 5006, Australia; [12]School of Paediatrics and Reproductive Health, University of Adelaide, Adelaide, SA 5005, Australia; [13]Division of Medical Genetics, Saitama Children's Medical Center, Saitama 339-8551, Japan; [14]Department of Genetic Counseling, Ochanomizu University, Tokyo 112-8610, Japan; [15]Department of Pediatrics Keio University School of Medicine, Tokyo 160-8582, Japan; [16]Division of Neonatal Intensive Care Unit, General Perinatal Medical Center, Wakayama Medical University, Wakayama 641-8510, Japan; [17]Department of Pediatrics, Jikei University School of Medicine, Tokyo 105-8461, Japan; [18]Department of Pediatrics, Niigata Graduate School of Medical and Dental Sciences, Niigata 951-8510, Japan; [19]Division of Cell Proliferation, United Centers for Advanced Research and Translational Medicine, Tohoku University Graduate School of Medicine, Sendai 980-8575, Japan; [20]National Research Institute for Child Health and Development, Tokyo 157-8535, Japan
*Correspondence: aokiy@med.tohoku.ac.jp
http://dx.doi.org/10.1016/j.ajhg.2013.05.021.

with Costello syndrome (MIM 218040) and cardiofaciocutaneous (CFC) syndrome (MIM 115150).

In 2001, Tartaglia et al. identified missense mutations in protein-tyrosine phosphatase, nonreceptor type 11 (*PTPN11* [MIM 176876]), which encodes the tyrosine phosphatase SHP-2 in 50% of individuals with Noonan syndrome.[5] In contrast, loss-of-function or dominant-negative mutations in *PTPN11* have been reported in individuals with Noonan syndrome with multiple lentigines[6] (formerly referred to as LEOPARD [multiple lentigines, electrocardiographic conduction abnormalities, ocular hypertelorism, pulmonic stenosis, abnormal genitalia, retardation of growth, and sensorineural deafness] syndrome [MIM 151100]). To date, germline mutations in *PTPN11*, *KRAS* (MIM 190070), *SOS1* (MIM 182530), *RAF1* (MIM 164760), and *NRAS* (MIM 164790) have been identified in individuals with Noonan syndrome[7–12] (NS1 [MIM 163950], NS3 [MIM 609942], NS4 [MIM 610733], NS5 [MIM 611553], and NS6 [MIM 613224]), and mutations in *SHOC2* (MIM 602775) and *CBL* (MIM 165360) have been identified in two Noonan-syndrome-like syndromes[13–16] (NSLH [MIM 607721] and NSLL [MIM 613563], respectively) (Figure S1, available online). Moreover, we and another group have identified germline mutations in *HRAS* (MIM 190020) in individuals with Costello syndrome[17] and germline mutations in *KRAS*, *BRAF* (MIM 164757), *MAP2K1* (MIM 176872), and *MAP2K2* (MIM 601263) in individuals with CFC syndrome.[18,19] Mutations in *BRAF* have been also identified in a small percentage of individuals with Noonan syndrome (NS7 [MIM 613706]). A line of studies have shown that a group of the above genetic disorders result from dysregulation of the RAS and downstream signaling cascade (RAS/MAPK pathway syndromes, or RASopathies).[20,21] Recently, mosaicism for *KRAS* and *HRAS* mutations has been reported in nevus sebaceous and Schimmelpenning syndrome,[22] further extending a spectrum of diseases with a dysregulated RAS/MAPK pathway.

To identify genetic causes of Noonan syndrome, we recruited 180 individuals with Noonan syndrome or a related phenotype; they were negative for all coding exons in *PTPN11*, *KRAS*, *HRAS*, and *SOS1*; exons 6 and 11–16 in *BRAF*; exons 7, 14, and 17 in *RAF1*; exons 2 and 3 in *MAP2K1* and *MAP2K2*; and exon 1 in *SHOC2*. Further genetic analysis has been conducted according to their first diagnoses.[17,23–29] This study was approved by the ethics committee of Tohoku University School of Medicine. We obtained informed consent from all subjects involved in the study. We sequenced the exomes of 14 individuals whose clinical manifestations had been confirmed to be consistent with Noonan syndrome by trained dysmorphologists. Targeted enrichment was performed with the Agilent SureSelect Human All Exon v.1 Kit for four individuals and with the SureSelect Human All Exon 50Mb kit for ten individuals. Exon-enriched DNA libraries from these 14 individuals were sequenced on the Illumina Hiseq 2000 for 91 bp (v.1 kit) or 101 bp (50Mb kit). The Burrows-Wheeler Aligner (BWA) was used to align the sequence reads to the human genome (UCSC Genome Browser hg19);[30] all BWA parameters were kept at the default settings. After the removal of duplicates from the alignments, realignment around known indels, recalibration, and SNP and indel calling were performed with the Genome Analysis Toolkit (v.1.5).[31] ANNOVAR was used for annotation against the RefSeq database and dbSNP.[32] We identified approximately 10,000 nonsynonymous, nonsense, and splice-site variations and coding indels per individual (Table S1). Filtering steps using variant databases (dbSNP132 and the 1000 Genome Project database) and in-house exome data were carried out, resulting in the identification of 122–282 variants per individual. By visual inspection of the generated data, four heterozygous *RIT1* (MIM 609591; RefSeq accession number NM_006912.5) variants (c.246T>G [p.Phe82Leu], c.265T>C [p.Tyr89His], c.270G>T [p.Met90Ile], and c.284G>C [p.Gly95Ala]) were found in four individuals. Sanger sequencing validated the heterozygous state of the four variants. We did not find any other strong candidate genes in the results of exome sequencing.

RIT1 shares approximately 50% sequence identity with RAS, has an additional N-terminal extension, and does not possess a C-terminal CAAX motif, a specific motif for post-translational modification.[33,34] *RIT1* is located in chromosomal region 1q22 and consists of six exons. We analyzed an additional 166 individuals diagnosed with Noonan syndrome or a related disorder but without mutations in known genes.[17,23–29] Sanger sequencing of all coding exons in *RIT1* in the 166 individuals showed that 13 in 166 individuals had changes. Combining with the 4 in 14 individuals from exome sequencing, a total of nine missense, nonsynonymous mutations were identified in 17 of 180 (9%) individuals who were suspected to have Noonan syndrome or a related disorder (Table 1 and Figures 1A–1L). The identified germline *RIT1* mutations encode alterations located in the G1 domain (c.104G>C [p.Ser35Thr]); the switch I region, involving the G2 domain (c.170C>G [p.Ala57Gly]); and the switch II region, corresponding to RAS (c.242A>G [p.Glu81Gly], c.244T>G [p.Phe82Val], c.246T>G [p.Phe82Leu], c.247A>C [p.Thr83Pro], c.265T>C [p.Tyr89His], c.270G>T [p.Met90Ile], and c.284G>C [p.Gly95Ala]) (Figure S2). Amino acids where alterations are located are conserved among species (Figure S3). The *RIT1* mutations encode alterations clustered in the switch II region. In contrast, *HRAS* germline mutations identified in Costello syndrome are clustered at codon 12 and 13 in the region encoding the G1 domain[17] (Figure 1M). Mutations in parents were not identified in seven families. These mutations are apparently de novo, but biologic confirmation of parentage was not performed. One mutation, c.104G>C, was inherited from a mother with a Noonan syndrome phenotype (Table 1). None of these mutations were identified in 480 controls.

To assess the functional consequences of *RIT1* mutations identified in affected individuals, we introduced a

Table 1. Mutations in *RIT1*, Family Status, and Heart Defects of Mutation-Positive Individuals

Subject	Exon	Nucleotide Change[a]	Amino Acid Change[b]	Father	Mother	HCM[c]	PS[c]	Other Heart Defects[c]
NS414	2	c.104G>C	p.Ser35Thr	WT	p.Ser35Thr	+	–	MVP, MR
KCC27	2	c.104G>C	p.Ser35Thr	NA	NA	+	+	–
NS43	4	c.170C>G	p.Ala57Gly	NA	NA	+	–	MR, TR
NS185	4	c.170C>G	p.Ala57Gly	NA	NA	+	+	ASD, PDA
NS216	4	c.170C>G	p.Ala57Gly	NA	NA	+	–	–
NS402	4	c.170C>G	p.Ala57Gly	WT	WT	+	+	–
NS168	5	c.242A>G	p.Glu81Gly	NA	NA	–	+	VSD
NS410	5	c.244T>G	p.Phe82Val	WT	WT	+	–	–
NS358	5	c.246T>G	p.Phe82Leu	WT	WT	–	+	ASD
NS465	5	c.246T>G	p.Phe82Leu	NA	NA	–	+	VSD
NS276	5	c.247A>C	p.Thr83Pro	WT	WT	+	+	PVC
KCC8	5	c.265T>C	p.Tyr89His	NA	NA	+	+	–
KCC38	5	c.270G>T	p.Met90Ile	WT	WT	+	+	ASD, VSD, PDA
NS234	5	c.284G>C	p.Gly95Ala	WT	WT	–	–	ASD
NS265	5	c.284G>C	p.Gly95Ala	WT	WT	+	+	–
Og22	5	c.284G>C	p.Gly95Ala	NA	NA	–	–	–
Og45	5	c.284G>C	p.Gly95Ala	NA	NA	+	+	ASD

PCR primers used for sequencing are shown in Table S3. Nucleotide changes are not located in CpG dinucleotides, suggesting that they exhibit baseline mutation rates with a phenotypic filtering effect and that only these mutations lead to this phenotype. Abbreviations are as follows: WT, wild-type; HCM, hypertrophic cardiomyopathy; PS, pulmonic stenosis; MVP, mitral valve prolapse; MR, mitral regurgitation; TR, tricuspid regurgitation; ASD, atrial septal defect; PDA, patent ductus arteriosus; VSD, ventricular septal defect; PVC, premature ventricular contraction; and NA, not available.
[a]RefSeq NM_006912.5.
[b]RefSeq NP_008843.1.
[c]HCM and heart anomalies were diagnosed by echocardiography.

single-base substitution (p.Ser35Thr, p.Ala57Gly, p.Glu81Gly, p.Phe82Leu, or p.Gly95Ala) identified in individuals with Noonan syndrome into a pCAGGS expression vector[36] harboring *RIT1* cDNA. As an experimental control, cDNAs harboring *RIT1* c.89G>T (p.Gly30Val), c.104G>C (p.Ser35Asn), and c.236A>T (p.Gln79Leu) and *Braf* c.1910T>A (p.Val637Glu) (RefSeq NM_139294), which corresponds to oncogenic p.Val600Glu in humans, were also generated. RIT1 p.Gly30Val and p.Gln79Leu correspond to oncogenic RAS alterations p.Gly12Val and p.Gln61Leu, respectively. We introduced pFR-luc, pFA2-Elk1, phRLnull-luc, and wild-type (WT) or mutant expression constructs of *RIT1* into NIH 3T3 cells to examine the transcriptional activation by ELK1,[18,33] a transcription factor that is activated by MAPK. The results revealed that compared with the WT cDNA, all *RIT1* mutations exhibited significant activation. RIT1 p.Gln79Leu, followed by p.Gly95Ala, p.Ala57Gly, p.Phe82Leu, and p.Glu81Gly, showed the highest ELK1 transactivation, as also shown in a past study[37] (Figure 2A). The c.104G>C (p.Ser35Thr) substitution was identified in two affected individuals. RIT1 p.Ser35Asn, which corresponds to dominant-negative alteration p.Ser17Asn in RAS, has been used as a dominant-negative substitution in cell experiments.[38] To examine the functional consequence of p.Ser35Thr, identified in affected individuals, we compared the ELK1 transactivation in cells expressing p.Ser35Thr and those expressing p.Ser35Asn. Enhanced ELK1 transactivation was observed in cells expressing p.Ser35Thr, but not in cells expressing p.Ser35Asn (Figure 2B). These results suggest that *RIT1* mutations identified in affected individuals were gain-of-function mutations.

RIT1 is expressed ubiquitously in embryonic and adult tissues.[33,34] *Rit1*-null mice have been shown to grow to adulthood without any apparent abnormalities;[39] hence, physiological roles of RIT1 in development remain unknown. To examine the developmental effect of identified mutations, we introduced mRNA of the WT and three *RIT1* mutations (c.236A>T [p.Gln79Leu], c.242A>G [p.Glu81Gly], and c.284G>C [p.Gly95Ala]) into 1-cell-stage zebrafish embryos and observed the phenotype at 11 hr postfertilization (hpf). An oval-shaped egg sack, a typical manifestation of the gastrulation defect, was observed in embryos expressing RIT1 alterations (Figure 3A). This characteristic shape change was also observed in zebrafish expressing gain-of-function mutations of human *NRAS*[40]. Next, we observed the phenotype at later stages (48–52 hpf) (Figure 3B and Figure S4). The introduction of the WT mRNA did not interfere with the normal development, resulting in generally normal morphology

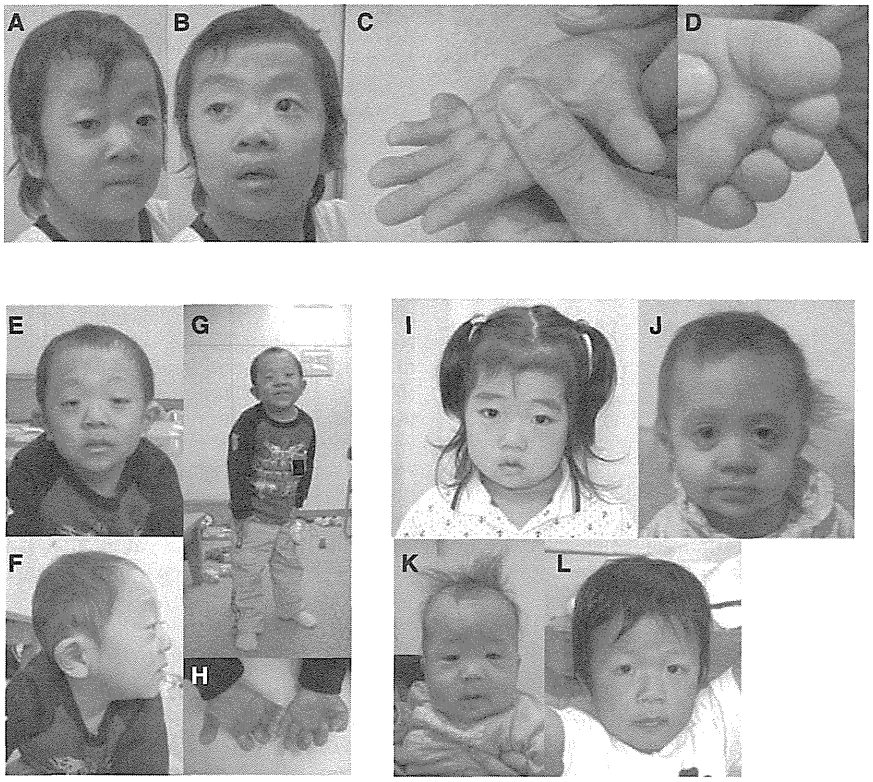

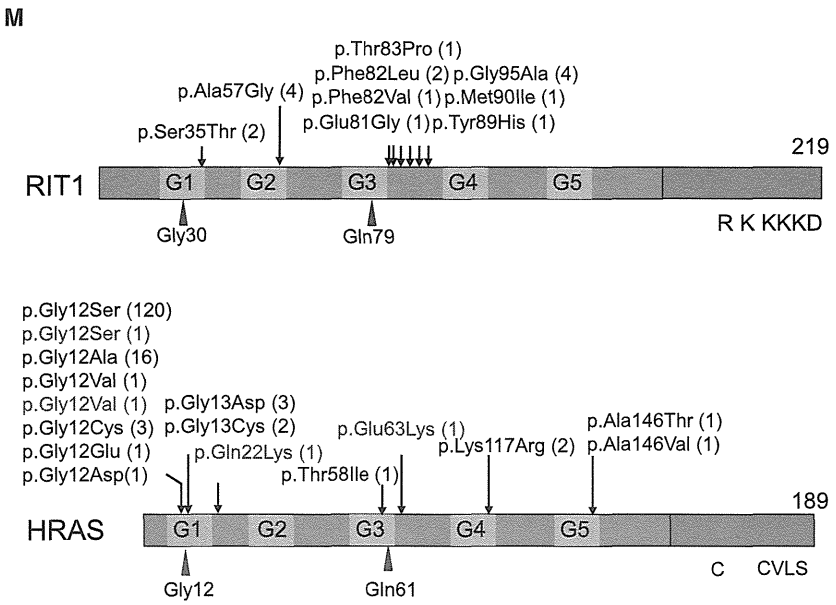

Figure 1. Photographs of Six Individuals in whom *RIT1* Mutations Were Identified
(A–D) KCC38 at 3 years of age. Broad forehead, sparse eyebrows, ptosis, hypertelorism, and hyperpigmentation were observed (A and B). Prominent finger pads were observed (C and D).
(E–H) NS358 at 4 years of age. Hypertelorism, epicanthus, sparse eyebrows, and low-set ears were observed.
(I) NS414 at 3 years of age.
(J) NS465 at 1 year of age.
(K) NS276 at 5 months.
(L) NS265 at 5 years of age.
(M) Structure and identified germline alterations in RIT1 and HRAS. HRAS alterations identified in individuals with Costello syndrome were described before[20] or shown in The RAS/MAPK Syndromes Homepage (see Web Resources). HRAS alterations identified in individuals with congenital myopathy with excess of muscle spindles[35] are indicated in purple.
We obtained specific consent for photographs from six individuals.

in 125/132 (94.7%) embryos; however, 7/132 (5.3%) embryos had limited mild craniofacial and heart abnormalities (Table 2). In contrast, a combined manifestation of craniofacial abnormalities, pericardial edema, and an elongated yolk sac was observed in 66.1%, 52.4%, and 40.5% of embryos expressing p.Gln79Leu, p.Glu81Gly, and p.Gly95Ala, respectively. Development was severely retarded in approximately 7% of embryos expressing RIT1 alterations; these embryos displayed the formation of a disorganized round body shape with a dysmorphic head and body trunk. In the head region, a hypoplastic brain, especially in the telencephalic area, was observed and resulted in misshapen morphology. In the ventral part of the head, the jaw structure was also hypoplastic, and the eyes were translocated medially. These morphological changes gave a cyclopia-like appearance. The ventral sides of the eyes were small, and coloboma along with a loss of pigment was evident (Figure 3B). These phenotypic changes are compatible with the gastrulation defect observed at 11 hpf (Figure 3A). Because the Fgf/Ras/MAPK signaling cascade plays an essential role in the convergent and extension cell movement during gastrulation,[41] perturbation by the RIT1 alterations could cause abnormal cell movement in the axial portions and thus lead to an elongated shape of the egg and the hypoplastic ventral side of the head. Detailed inspection of the morphology in mutant-injected embryos revealed abnormal cardiogenesis, namely, incomplete looping, hypoplastic chambers, and stagnation of blood flow in the yolk sac (Figure 3B). Although the atrium of these hearts beat regularly, the ventricle seemed to twitch passively by the contraction of the atrium (Movies S1, S2, S3, S4, S5, and S6). These results indicate that activating mutations in *RIT1* induce abnormal craniofacial and heart defects in zebrafish.

RIT1-mutation-positive individuals showed a distinct facial appearance, congenital heart defects, and skeletal

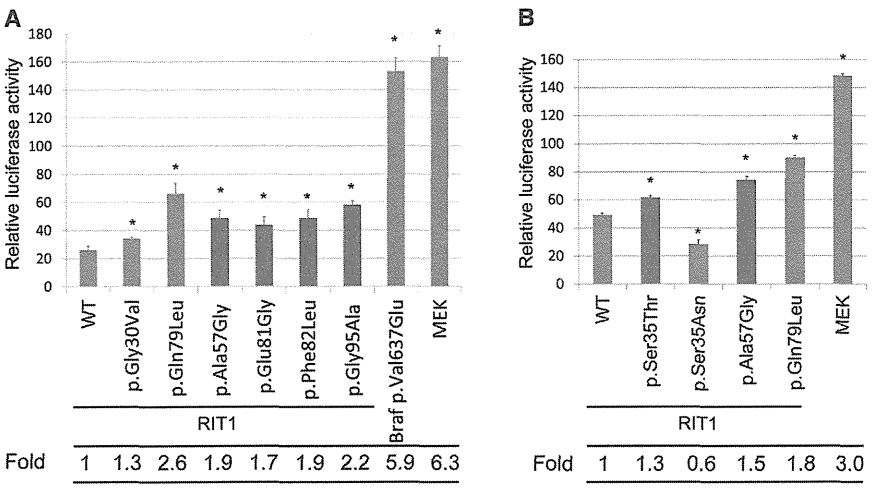

Figure 2. Stimulation of ELK Transcription in NIH 3T3 Cells Expressing *RIT1* Germline Mutations

(A) The ELK1-GAL4 vector and the GAL4 luciferase *trans*-reporter vector were transiently transfected with various *RIT1* germline mutations and activating mutations in *BRAF* and *MAP2K1* in NIH 3T3 cells. c.1910T>A (p.Val637Glu) in mouse *Braf* corresponds to oncogenic c.1799T>A (p.Val600Glu) in human *BRAF*. Relative luciferase activity was calculated by normalization to the activity of a cotransfected control vector, phRLnull-luc, containing distinguishable *R. reniformis* luciferase.

(B) ELK1 transactivation in cells expressing p.Ser35Thr, identified in individuals with Noonan syndrome, and p.Ser35Asn, were examined. p.Ser35Asn corresponds to dominant-negative alteration p.Ser17Asn in RAS.

Results are expressed as the means of quadruplicate (A) and triplicate (B) samples. Error bars represent the SDs of mean values. Red bars indicate germline *RIT1* mutations identified in Noonan syndrome. The following abbreviation is used: WT, wild-type. *$p < 0.01$ by t test.

abnormalities and were diagnosed with Noonan syndrome by diagnostic criteria developed by van der Burgt (Figures 1A–1L and Table 1).[4] Two individuals (NS358 and KCC38) were suspected to have CFC syndrome in the infantile period because of curly, sparse hair, a high cranial vault, and hypoplasia of the supraorbital ridges. Nine individuals showed perinatal abnormality, including polyhydramnios, nuchal translucency, and chylothorax (Table S2). It is of note that one individual (Og45) showing severe pleural effusion, hypertrophic cardiomyopathy, and hepatomegaly that ended in severe body edema and compromised circulation died 53 days after birth. Seven individuals showed high birth weight, probably as a result of subcutaneous edema, which is a typical manifestation observed in individuals with Noonan syndrome.[4] Out of 17 affected individuals, 16 (94%) had heart defects (Table 1): hypertrophic cardiomyopathy (HCM) in 12 (71%) individuals, pulmonary stenosis in 11 (65%) individuals, and atrial septal defects in 5 (29%) individuals. The incidence of pulmonic stenosis and mild cognitive defects is close to the overall incidence of these features in Noonan syndrome cohorts. By contrast, the incidence of HCM is far greater than in individuals with Noonan syndrome overall (25/118 in Noonan syndrome[42] versus 12/17 in individuals with *RIT1* mutations; $p < 0.0001$ by Fisher's exact test). It is of note that a high frequency of HCM (70%) was also reported in individuals with *RAF1* mutations.[10,11,24] It is possible that RIT1 interacts with RAF1 and that gain-of-function mutations in *RIT1* and *RAF1* exert similar effects in heart development.

Somatic alterations in classical RAS have been identified in approximately 30% of tumors.[43] Noonan syndrome and related disorders confer an increased risk of developing malignant tumors.[20,44] In a summary of the literature, it has been reported that 45 of 1,151 (3.9%) individuals with Noonan syndrome (but with an unknown mutation status) developed malignant tumors.[44] Since molecular analysis became available, gene-specific association with malignant tumors has been revealed. The association with JMML, a myeloproliferative disorder characterized by the excessive production of myelomonocytic cells, has been reported in individuals with *PTPN11*, *CBL*, and *KRAS* mutations. Recent reports showed that two individuals with *SOS1* mutations developed embryonal rhabdomyosarcoma.[45,46] A somatic *RIT1* variant, c.270G>A (p.Met90Ile), has been identified in lung cancer (COSMIC database). In the present cohort, 1 (NS168) of 17 individuals with *RIT1* c.242A>G (p.Glu81Gly) developed acute lymphoblastic leukemia at the age of 5 years. The child was treated by a standard protocol and has remained in complete remission. Examining whether gain-of-function mutations in *RIT1* cause tumorigenesis will require further study.

RIT1 has been isolated as a cDNA encoding highly conserved G3 and G4 domains of RAS proteins[33] or identified as a gene encoding a protein related to *Drosophila Ric*, a calmodulin-binding RAS-related GTPase.[34] RIT1 p.Gln79Leu, which corresponds to RAS p.Gln61Leu, is implicated in transforming NIH 3T3 cells, neurite outgrowth in neuronal cells, and the activation of ERK and p38 MAPK in a cell-specific manner.[37,38,47] In this study, enhanced ELK1 transactivation was observed in cells expressing mutant *RIT1* cDNAs. Previous studies showed that enhanced ELK transactivation was observed in NIH 3T3 cells expressing *HRAS*, *KRAS*, *BRAF*, and *RAF1* mutations identified in individuals with Costello, CFC, and Noonan syndromes.[17,18,24] Gastrulation defects observed in zebrafish embryos expressing RIT1 alterations (p.Glu81Gly, p.Gly95Ala, or p.Gln79Leu) were also reported in zebrafish embryos expressing an activating mutation in *NRAS*, *BRAF*, *MAP2K1*, or *MAP2K2*.[40,48] Taken together, these

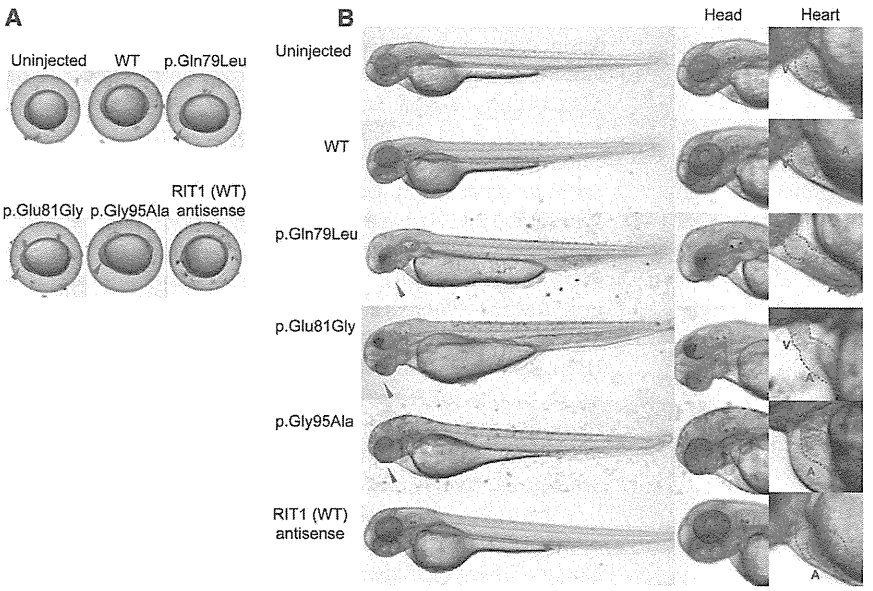

Figure 3. Morphology of Embryos Injected with the WT or Mutant *RIT1* mRNA
In vitro transcription of each mRNA was performed with the mMESSAGE mMACHINE kit (Applied Biosystems) according to the manufacturer's instructions. Synthesized mRNAs were purified with G-50 Micro Columns (GE Healthcare) and subsequently adjusted to a 300 ng/μl concentration for microinjection. Approximately 1 nl (300 pg) of RNA in water with 0.2% phenol red was injected into the cytoplasm of 1-cell-stage zebrafish embryos. Injected embryos were incubated at 28°C until observation.
(A) At 11 hpf, the shapes of the embryos injected with the WT sense or antisense mRNA were round, a normal morphology as observed in the uninjected embryos. In contrast, embryos expressing mutations (c.236A>T [p.Gln79Leu], c.242A>G [p.Glu81Gly], and c.284G>C [p.Gly95Ala]) are oval and compressed along the dorsal-ventral axis, indicative of a gastrulation defect. Note that cells have a hump in the head region at the anterior end of the body axis, the earliest manifestation of a craniofacial defect.
(B) Lateral views at 48 hpf are shown. Embryos expressing mutations (c.236A>T [p.Gln79Leu], c.242A>G [p.Glu81Gly], and c.284G>C [p.Gly95Ala]) formed swollen yolk sacs equally along the anterior posterior axis but did not show narrowing in the caudal half, which was clearly visible in the uninjected embryos and in those injected with the WT sense or antisense mRNA. In the craniofacial area, misshapen head and jaw structures and small eyes with hypoplasia on the ventral side were observed (middle panel); these phenotypes are consistent with the gastrulation defect. Shapes of the hearts (highlighted by red dotted lines) are shown in the right panel at a higher magnification. Normal looping of the heart tube and correct formation of two distinct chambers are observed in embryos injected with the WT sense or antisense mRNA. When mutations (c.236A>T [p.Gln79Leu], c.242A>G [p.Glu81Gly], and c.284G>C [p.Gly95Ala]) were expressed, looping was incomplete, resulting in stretched straight heart tubes. Constrictions at the atrial-ventricular canal are obscure, and the heart chambers are hypoplastic. Abbreviations are as follows: A, atrium; and V, ventricle.

results indicate that gain-of-function mutations in *RIT1* cause Noonan syndrome and show a similar effect to mutations in other RASopathy-related genes in human development.

Herein, we used whole-exome sequencing to identify germline *RIT1* mutations in individuals with Noonan syndrome, a disorder of the RASopathies. Mutations in *PTPN11*, *SOS1*, *RAF1*, *KRAS*, *BRAF*, and *NRAS* have been identified in 41%, 11%, 5%, 1%, 0.8%, and 0.2% of all cases, respectively,[3] and thus the frequency of *RIT1* mutations in Noonan syndrome might be similar to that of *RAF1* mutations. Our findings will improve diagnostic accuracy of Noonan syndrome and provide a clue to understanding the disorder's pathogenesis, including therapeutic approaches.

Supplemental Data

Supplemental Data include four figures, three tables, and six movies and can be found with this article online at http://www.cell.com/AJHG/.

Acknowledgments

The authors thank the families and the doctors who participated in this study. We are grateful to Jun-ichi Miyazaki at Osaka University for supplying the pCAGGS expression vector. We thank Yoko Narumi, Tomoko Kobayashi, Shoko Komatsuzaki, Yu Abe, Yuka Saito, Rumiko Izumi, Mitsuji Moriya, and Masako Yaoita for contributing to routine diagnostic work and Yoko Tateda, Kumi Kato, and Riyo Takahashi for their technical assistance. We are grateful to Eric Haan for sending samples of Noonan syndrome

Table 2. Morphologic Abnormality at 48–52 hpf of Zebrafish Embryos Injected with WT or Mutant RNA at the 1-Cell Stage

	No Abnormalities	Heart and Facial Abnormalities[a]	Severely Disorganized[b]	Total Number of Embryos
WT	125	7 (5.3%)	0 (0%)	132
p.Gln79Leu	31	78 (66.1%)	9 (7.6%)	118
p.Glu81Gly	42	55 (52.4%)	8 (7.6%)	105
p.Gly95Ala	44	34 (40.5%)	6 (7.1%)	84

[a]Craniofacial abnormalities, pericardial heart edema, and an elongated yolk sac were observed.
[b]Disorganized round body shape with a dysmorphic head and body trunk as shown in Figure S4.

and related disorders. We also acknowledge the support of the Biomedical Research Core of Tohoku University Graduate School of Medicine. This work was supported by the Funding Program for the Next Generation of World-Leading Researchers (NEXT Program) from the Ministry of Education, Culture, Sports, Science, and Technology of Japan (MEXT) to Y.A. (LS004), by Grants-in-Aids from MEXT, from the Japan Society for the Promotion of Science, and from the Ministry of Health, Labor, and Welfare to Y.M. and T.N. This work was supported in part by the National Cancer Center Research and Development Fund (23-22-11).

Received: April 23, 2013
Revised: May 19, 2013
Accepted: May 23, 2013
Published: June 20, 2013

Web Resources

The URLs for data presented herein are as follows:

Catalogue of Somatic Mutations in Cancer (COSMIC), http://www.sanger.ac.uk/genetics/CGP/cosmic/

Online Mendelian Inheritance in Man (OMIM), http://www.omim.org

RefSeq, http://www.ncbi.nlm.nih.gov/RefSeq

The RAS/MAPK Syndromes Homepage, http://www.medgen.med.tohoku.ac.jp/RasMapk%20syndromes.html

References

1. Takai, Y., Sasaki, T., and Matozaki, T. (2001). Small GTP-binding proteins. Physiol. Rev. *81*, 153–208.
2. Giehl, K. (2005). Oncogenic Ras in tumour progression and metastasis. Biol. Chem. *386*, 193–205.
3. Romano, A.A., Allanson, J.E., Dahlgren, J., Gelb, B.D., Hall, B., Pierpont, M.E., Roberts, A.E., Robinson, W., Takemoto, C.M., and Noonan, J.A. (2010). Noonan syndrome: clinical features, diagnosis, and management guidelines. Pediatrics *126*, 746–759.
4. van der Burgt, I. (2007). Noonan syndrome. Orphanet J. Rare Dis. *2*, 4.
5. Tartaglia, M., Mehler, E.L., Goldberg, R., Zampino, G., Brunner, H.G., Kremer, H., van der Burgt, I., Crosby, A.H., Ion, A., Jeffery, S., et al. (2001). Mutations in PTPN11, encoding the protein tyrosine phosphatase SHP-2, cause Noonan syndrome. Nat. Genet. *29*, 465–468.
6. Digilio, M.C., Conti, E., Sarkozy, A., Mingarelli, R., Dottorini, T., Marino, B., Pizzuti, A., and Dallapiccola, B. (2002). Grouping of multiple-lentigines/LEOPARD and Noonan syndromes on the PTPN11 gene. Am. J. Hum. Genet. *71*, 389–394.
7. Schubbert, S., Zenker, M., Rowe, S.L., Böll, S., Klein, C., Bollag, G., van der Burgt, I., Musante, L., Kalscheuer, V., Wehner, L.E., et al. (2006). Germline KRAS mutations cause Noonan syndrome. Nat. Genet. *38*, 331–336.
8. Roberts, A.E., Araki, T., Swanson, K.D., Montgomery, K.T., Schiripo, T.A., Joshi, V.A., Li, L., Yassin, Y., Tamburino, A.M., Neel, B.G., and Kucherlapati, R.S. (2007). Germline gain-of-function mutations in SOS1 cause Noonan syndrome. Nat. Genet. *39*, 70–74.
9. Tartaglia, M., Pennacchio, L.A., Zhao, C., Yadav, K.K., Fodale, V., Sarkozy, A., Pandit, B., Oishi, K., Martinelli, S., Schackwitz, W., et al. (2007). Gain-of-function SOS1 mutations cause a distinctive form of Noonan syndrome. Nat. Genet. *39*, 75–79.
10. Pandit, B., Sarkozy, A., Pennacchio, L.A., Carta, C., Oishi, K., Martinelli, S., Pogna, E.A., Schackwitz, W., Ustaszewska, A., Landstrom, A., et al. (2007). Gain-of-function RAF1 mutations cause Noonan and LEOPARD syndromes with hypertrophic cardiomyopathy. Nat. Genet. *39*, 1007–1012.
11. Razzaque, M.A., Nishizawa, T., Komoike, Y., Yagi, H., Furutani, M., Amo, R., Kamisago, M., Momma, K., Katayama, H., Nakagawa, M., et al. (2007). Germline gain-of-function mutations in RAF1 cause Noonan syndrome. Nat. Genet. *39*, 1013–1017.
12. Cirstea, I.C., Kutsche, K., Dvorsky, R., Gremer, L., Carta, C., Horn, D., Roberts, A.E., Lepri, F., Merbitz-Zahradnik, T., König, R., et al. (2010). A restricted spectrum of NRAS mutations causes Noonan syndrome. Nat. Genet. *42*, 27–29.
13. Cordeddu, V., Di Schiavi, E., Pennacchio, L.A., Ma'ayan, A., Sarkozy, A., Fodale, V., Cecchetti, S., Cardinale, A., Martin, J., Schackwitz, W., et al. (2009). Mutation of SHOC2 promotes aberrant protein N-myristoylation and causes Noonan-like syndrome with loose anagen hair. Nat. Genet. *41*, 1022–1026.
14. Loh, M.L., Sakai, D.S., Flotho, C., Kang, M., Fliegauf, M., Archambeault, S., Mullighan, C.G., Chen, L., Bergstraesser, E., Bueso-Ramos, C.E., et al. (2009). Mutations in CBL occur frequently in juvenile myelomonocytic leukemia. Blood *114*, 1859–1863.
15. Niemeyer, C.M., Kang, M.W., Shin, D.H., Furlan, I., Erlacher, M., Bunin, N.J., Bunda, S., Finklestein, J.Z., Sakamoto, K.M., Gorr, T.A., et al. (2010). Germline CBL mutations cause developmental abnormalities and predispose to juvenile myelomonocytic leukemia. Nat. Genet. *42*, 794–800.
16. Pérez, B., Mechinaud, F., Galambrun, C., Ben Romdhane, N., Isidor, B., Philip, N., Derain-Court, J., Cassinat, B., Lachenaud, J., Kaltenbach, S., et al. (2010). Germline mutations of the CBL gene define a new genetic syndrome with predisposition to juvenile myelomonocytic leukaemia. J. Med. Genet. *47*, 686–691.
17. Aoki, Y., Niihori, T., Kawame, H., Kurosawa, K., Ohashi, H., Tanaka, Y., Filocamo, M., Kato, K., Suzuki, Y., Kure, S., and Matsubara, Y. (2005). Germline mutations in HRAS proto-oncogene cause Costello syndrome. Nat. Genet. *37*, 1038–1040.
18. Niihori, T., Aoki, Y., Narumi, Y., Neri, G., Cavé, H., Verloes, A., Okamoto, N., Hennekam, R.C., Gillessen-Kaesbach, G., Wieczorek, D., et al. (2006). Germline KRAS and BRAF mutations in cardio-facio-cutaneous syndrome. Nat. Genet. *38*, 294–296.
19. Rodriguez-Viciana, P., Tetsu, O., Tidyman, W.E., Estep, A.L., Conger, B.A., Cruz, M.S., McCormick, F., and Rauen, K.A. (2006). Germline mutations in genes within the MAPK pathway cause cardio-facio-cutaneous syndrome. Science *311*, 1287–1290.
20. Aoki, Y., Niihori, T., Narumi, Y., Kure, S., and Matsubara, Y. (2008). The RAS/MAPK syndromes: novel roles of the RAS pathway in human genetic disorders. Hum. Mutat. *29*, 992–1006.
21. Tidyman, W.E., and Rauen, K.A. (2009). The RASopathies: developmental syndromes of Ras/MAPK pathway dysregulation. Curr. Opin. Genet. Dev. *19*, 230–236.
22. Groesser, L., Herschberger, E., Ruetten, A., Ruivenkamp, C., Lopriore, E., Zutt, M., Langmann, T., Singer, S., Klingseisen, L., Schneider-Brachert, W., et al. (2012). Postzygotic HRAS and KRAS mutations cause nevus sebaceous and Schimmelpenning syndrome. Nat. Genet. *44*, 783–787.

23. Abe, Y., Aoki, Y., Kuriyama, S., Kawame, H., Okamoto, N., Kurosawa, K., Ohashi, H., Mizuno, S., Ogata, T., Kure, S., et al.; Costello and CFC syndrome study group in Japan. (2012). Prevalence and clinical features of Costello syndrome and cardio-facio-cutaneous syndrome in Japan: findings from a nationwide epidemiological survey. Am. J. Med. Genet. A. *158A*, 1083–1094.
24. Kobayashi, T., Aoki, Y., Niihori, T., Cavé, H., Verloes, A., Okamoto, N., Kawame, H., Fujiwara, I., Takada, F., Ohata, T., et al. (2010). Molecular and clinical analysis of RAF1 in Noonan syndrome and related disorders: dephosphorylation of serine 259 as the essential mechanism for mutant activation. Hum. Mutat. *31*, 284–294.
25. Komatsuzaki, S., Aoki, Y., Niihori, T., Okamoto, N., Hennekam, R.C., Hopman, S., Ohashi, H., Mizuno, S., Watanabe, Y., Kamasaki, H., et al. (2010). Mutation analysis of the SHOC2 gene in Noonan-like syndrome and in hematologic malignancies. J. Hum. Genet. *55*, 801–809.
26. Narumi, Y., Aoki, Y., Niihori, T., Neri, G., Cavé, H., Verloes, A., Nava, C., Kavamura, M.I., Okamoto, N., Kurosawa, K., et al. (2007). Molecular and clinical characterization of cardio-facio-cutaneous (CFC) syndrome: overlapping clinical manifestations with Costello syndrome. Am. J. Med. Genet. A. *143A*, 799–807.
27. Narumi, Y., Aoki, Y., Niihori, T., Sakurai, M., Cavé, H., Verloes, A., Nishio, K., Ohashi, H., Kurosawa, K., Okamoto, N., et al. (2008). Clinical manifestations in patients with SOS1 mutations range from Noonan syndrome to CFC syndrome. J. Hum. Genet. *53*, 834–841.
28. Niihori, T., Aoki, Y., Okamoto, N., Kurosawa, K., Ohashi, H., Mizuno, S., Kawame, H., Inazawa, J., Ohura, T., Arai, H., et al. (2011). HRAS mutants identified in Costello syndrome patients can induce cellular senescence: possible implications for the pathogenesis of Costello syndrome. J. Hum. Genet. *56*, 707–715.
29. Saito, Y., Aoki, Y., Muramatsu, H., Makishima, H., Maciejewski, J.P., Imaizumi, M., Rikiishi, T., Sasahara, Y., Kure, S., Niihori, T., et al. (2012). Casitas B-cell lymphoma mutation in childhood T-cell acute lymphoblastic leukemia. Leuk. Res. *36*, 1009–1015.
30. Li, H., and Durbin, R. (2009). Fast and accurate short read alignment with Burrows-Wheeler transform. Bioinformatics *25*, 1754–1760.
31. McKenna, A., Hanna, M., Banks, E., Sivachenko, A., Cibulskis, K., Kernytsky, A., Garimella, K., Altshuler, D., Gabriel, S., Daly, M., and DePristo, M.A. (2010). The Genome Analysis Toolkit: a MapReduce framework for analyzing next-generation DNA sequencing data. Genome Res. *20*, 1297–1303.
32. Wang, K., Li, M., and Hakonarson, H. (2010). ANNOVAR: functional annotation of genetic variants from high-throughput sequencing data. Nucleic Acids Res. *38*, e164.
33. Lee, C.H., Della, N.G., Chew, C.E., and Zack, D.J. (1996). Rin, a neuron-specific and calmodulin-binding small G-protein, and Rit define a novel subfamily of ras proteins. J. Neurosci. *16*, 6784–6794.
34. Wes, P.D., Yu, M., and Montell, C. (1996). RIC, a calmodulin-binding Ras-like GTPase. EMBO J. *15*, 5839–5848.
35. van der Burgt, I., Kupsky, W., Stassou, S., Nadroo, A., Barroso, C., Diem, A., Kratz, C.P., Dvorsky, R., Ahmadian, M.R., and Zenker, M. (2007). Myopathy caused by HRAS germline mutations: implications for disturbed myogenic differentiation in the presence of constitutive HRas activation. J. Med. Genet. *44*, 459–462.
36. Niwa, H., Yamamura, K., and Miyazaki, J. (1991). Efficient selection for high-expression transfectants with a novel eukaryotic vector. Gene *108*, 193–199.
37. Rusyn, E.V., Reynolds, E.R., Shao, H., Grana, T.M., Chan, T.O., Andres, D.A., and Cox, A.D. (2000). Rit, a non-lipid-modified Ras-related protein, transforms NIH3T3 cells without activating the ERK, JNK, p38 MAPK or PI3K/Akt pathways. Oncogene *19*, 4685–4694.
38. Shi, G.X., and Andres, D.A. (2005). Rit contributes to nerve growth factor-induced neuronal differentiation via activation of B-Raf-extracellular signal-regulated kinase and p38 mitogen-activated protein kinase cascades. Mol. Cell. Biol. *25*, 830–846.
39. Cai, W., Rudolph, J.L., Harrison, S.M., Jin, L., Frantz, A.L., Harrison, D.A., and Andres, D.A. (2011). An evolutionarily conserved Rit GTPase-p38 MAPK signaling pathway mediates oxidative stress resistance. Mol. Biol. Cell *22*, 3231–3241.
40. Runtuwene, V., van Eekelen, M., Overvoorde, J., Rehmann, H., Yntema, H.G., Nillesen, W.M., van Haeringen, A., van der Burgt, I., Burgering, B., and den Hertog, J. (2011). Noonan syndrome gain-of-function mutations in NRAS cause zebrafish gastrulation defects. Dis Model Mech *4*, 393–399.
41. Fürthauer, M., Van Celst, J., Thisse, C., and Thisse, B. (2004). Fgf signalling controls the dorsoventral patterning of the zebrafish embryo. Development *131*, 2853–2864.
42. Burch, M., Sharland, M., Shinebourne, E., Smith, G., Patton, M., and McKenna, W. (1993). Cardiologic abnormalities in Noonan syndrome: phenotypic diagnosis and echocardiographic assessment of 118 patients. J. Am. Coll. Cardiol. *22*, 1189–1192.
43. Schubbert, S., Shannon, K., and Bollag, G. (2007). Hyperactive Ras in developmental disorders and cancer. Nat. Rev. Cancer *7*, 295–308.
44. Kratz, C.P., Rapisuwon, S., Reed, H., Hasle, H., and Rosenberg, P.S. (2011). Cancer in Noonan, Costello, cardiofaciocutaneous and LEOPARD syndromes. Am. J. Med. Genet. C. Semin. Med. Genet. *157*, 83–89.
45. Denayer, E., Devriendt, K., de Ravel, T., Van Buggenhout, G., Smeets, E., Francois, I., Sznajer, Y., Craen, M., Leventopoulos, G., Mutesa, L., et al. (2010). Tumor spectrum in children with Noonan syndrome and SOS1 or RAF1 mutations. Genes Chromosomes Cancer *49*, 242–252.
46. Jongmans, M.C.J., Hoogerbrugge, P.M., Hilkens, L., Flucke, U., van der Burgt, I., Noordam, K., Ruiterkamp-Versteeg, M., Yntema, H.G., Nillesen, W.M., Ligtenberg, M.J.L., et al. (2010). Noonan syndrome, the SOS1 gene and embryonal rhabdomyosarcoma. Genes Chromosomes Cancer *49*, 635–641.
47. Hynds, D.L., Spencer, M.L., Andres, D.A., and Snow, D.M. (2003). Rit promotes MEK-independent neurite branching in human neuroblastoma cells. J. Cell Sci. *116*, 1925–1935.
48. Anastasaki, C., Estep, A.L., Marais, R., Rauen, K.A., and Patton, E.E. (2009). Kinase-activating and kinase-impaired cardio-facio-cutaneous syndrome alleles have activity during zebrafish development and are sensitive to small molecule inhibitors. Hum. Mol. Genet. *18*, 2543–2554.

Journal of Human Genetics (2013) 58, 259–266

www.nature.com/jhg

ORIGINAL ARTICLE

Exome sequencing identifies a novel *TTN* mutation in a family with hereditary myopathy with early respiratory failure

Rumiko Izumi[1,2], Tetsuya Niihori[1], Yoko Aoki[1], Naoki Suzuki[2], Masaaki Kato[2], Hitoshi Warita[2], Toshiaki Takahashi[3], Maki Tateyama[2], Takeshi Nagashima[4], Ryo Funayama[4], Koji Abe[5], Keiko Nakayama[4], Masashi Aoki[2] and Yoichi Matsubara[1]

Myofibrillar myopathy (MFM) is a group of chronic muscular disorders that show the focal dissolution of myofibrils and accumulation of degradation products. The major genetic basis of MFMs is unknown. In 1993, our group reported a Japanese family with dominantly inherited cytoplasmic body myopathy, which is now included in MFM, characterized by late-onset chronic progressive distal muscle weakness and early respiratory failure. In this study, we performed linkage analysis and exome sequencing on these patients and identified a novel c.90263G>T mutation in the *TTN* gene (NM_001256850). During the course of our study, another groups reported three mutations in *TTN* in patients with hereditary myopathy with early respiratory failure (HMERF, MIM #603689), which is characterized by overlapping pathologic findings with MFMs. Our patients were clinically compatible with HMERF. The mutation identified in this study and the three mutations in patients with HMERF were located on the A-band domain of titin, suggesting a strong relationship between mutations in the A-band domain of titin and HMERF. Mutation screening of *TTN* has been rarely carried out because of its huge size, consisting of 363 exons. It is possible that focused analysis of *TTN* may detect more mutations in patients with MFMs, especially in those with early respiratory failure.
Journal of Human Genetics (2013) **58,** 259–266; doi:10.1038/jhg.2013.9; published online 28 February 2013

Keywords: A-band; cytoplasmic body; Fn3 domain; hereditary myopathy with early respiratory failure; HMERF; myofibrillar myopathy; titin; *TTN*

INTRODUCTION

Myofibrillar myopathies (MFMs) were proposed in 1996 as a group of chronic muscular disorders characterized by common morphologic features observed on muscle histology, which showed the focal dissolution of myofibrils followed by the accumulation of products of the degradative process.[1] The clinical phenotype of MFM is characterized by slowly progressive muscle weakness that can involve proximal or distal muscles, with onset in adulthood in most cases. However, other phenotypes are highly variable. Although 20% of patients with MFMs have been revealed to have mutations in *DES*, *CRYAB*, *MYOT*, *LDB* (*ZASP*), *FLNC* or *BAG3*, the major genetic basis of MFMs remains to be elucidated.

Respiratory weakness is one of the symptoms of MFMs. The early or initial presentation of respiratory failure is not a common manifestation of MFMs as a whole, and there are limited reports regarding a fraction of patients with *DES*,[2] *MYOT*[3] or *CRYAB*[4] mutation. In 1993, our group reported a Japanese family with dominantly inherited cytoplasmic body (CB) myopathy,[5] which is now included in MFM. Currently, this family includes 20 patients in five successive generations who show almost homogeneous clinical features characterized by chronic progressive distal muscle weakness and early respiratory failure. However, the underlying genetic etiology in this family was unknown. The aim of this study was to determine the genetic cause in this family. To identify the responsible genetic mutation, we performed linkage analysis and whole-exome sequencing.

MATERIALS AND METHODS

This study was approved by the Ethics Committee of the Tohoku University School of Medicine, and all individuals gave their informed consent before their inclusion in the study.

[1]Department of Medical Genetics, Tohoku University School of Medicine, Sendai, Japan; [2]Department of Neurology, Tohoku University School of Medicine, Sendai, Japan; [3]Department of Neurology and Division of Clinical Research, National Hospital Organization Nishitaga National Hospital, Sendai, Japan; [4]Division of Cell Proliferation, United Centers for Advanced Research and Translational Medicine, Tohoku University Graduate School of Medicine, Sendai, Japan and [5]Department of Neurology, Okayama University Medical School, Okayama, Japan
Correspondence: Dr Y Aoki, Department of Medical Genetics, Tohoku University School of Medicine, 1-1 Seiryo-machi, Aoba-ku, Sendai 980-8574, Japan.
E-mail: aokiy@med.tohoku.ac.jp
or Professor M Aoki, Department of Neurology, Tohoku University School of Medicine, 1-1 Seiryo-machi, Aoba-ku, Sendai 980-8574, Japan.
E-mail: aokim@med.tohoku.ac.jp
Received 23 October 2012; revised 9 January 2013; accepted 10 January 2013; published online 28 February 2013

Clinical information on the family

This family includes 20 patients (13 males and 7 females) in five successive generations (Figure 1). The family is of Japanese ancestry, and no consanguineous or international mating was found. Of all patients, seven underwent a muscle biopsy, and two were autopsied. All of the histological findings were compatible with MFM (see clinical data).

The age of onset ranged from 27–45 years. The most common presenting symptom was foot drop. At the initial evaluations, muscle weakness was primarily distributed in the ankle dorsiflexors and finger extensors. The patients were generally built and showed no other extramuscular abnormalities. In addition to this chronic progressive distal muscle weakness, respiratory distress occurred between 0 and 7 years from the initial onset (average 3.8 years) in seven patients (IV-9, V-2, A, B, E, H, and J) with adequate clinical information. Two patients who had not had any respiratory care died of respiratory failure approximately a decade from the initial onset. The other patients have been alive for more than 10 years (maximum 18 years) but require nocturnal non-invasive positive pressure ventilation. They were 37–58 years of age as of 2012 and able to walk independently with or without a simple walking aid. Although the time at which patients recognized dysphagia or dysarthria varied between 1 to more than 10 years from the initial onset, decreased bulbar functions had been noted at the initial evaluation in most cases. Cardiac function was normally maintained in all patients of the family.

Clinical data

The level of serum creatine kinase was normal or mildly elevated. Electromyography of affected muscles showed a chronic myogenic pattern, and the nerve conduction study did not suggest any neuropathic involvement. Muscle imaging showed focal atrophy in the tibialis anterior, tibialis posterior, extensor hallucis and digitorum longus, peroneal and semitendinosus muscle on initial assessment (Figure 2A), and atrophy became clear in cervical muscles, shoulder girdles, intercostals and proximal limb muscles in the following several years. Upon muscle biopsy, the most common finding was numerous cytoplasmic bodies (CBs), which were found on 7.3% of myofibers in the tibialis anterior of individual E (Figure 2B (a–c)) and 50–80% of intercostals in other cases.[5] Other nonspecific findings were increased variability in the size of myofibers, central nuclei and rimmed vacuoles observed on a few fibers. No strong immunoreaction of desmin was seen in the CBs (Figure 2B (d, e)). An electron microscope examination showed that the regular sarcoplasmic pattern was replaced by abnormal fine filamentous structures, which seemed to attach to the Z-band. CBs were also found in almost all skeletal muscles and some smooth muscles in autopsied cases.[5] Cardiac myofibers also contained numerous CBs in one of the autopsied cases (V-2),[5] although the patient did not present any cardiac complication. The sequence analysis of the coding regions and flanking introns of *DES* and *MYOT* showed no pathogenic mutation in individual E. An array comparative genomic hybridization performed with the Agilent SurePrint G3 Human CGH 1M microarray format in individual A did not reveal any aberrations of genomic copy number.

Linkage analysis

DNA was extracted by standard methods. Linkage analysis was performed on nine family members (A–I in Figure 1; four of them were affected, and the others were unaffected) through genotyping using an Illumina Human Omni 2.5 BeadChip (Illumina, San Diego, CA, USA). We chose single-nucleotide polymorphisms (SNPs) that satisfied all of the following criteria: (1) autosomal SNPs whose allele frequencies were available from the HapMap project (http://hapmap.ncbi.nlm.nih.gov/), (2) SNPs that were not monomorphic among members and (3) SNPs that were not in strong linkage disequilibrium with neighboring SNPs (r2 values <0.9). Then, we selected the first five SNPs from each position of integer genetic distance from SNPs that met the above criteria for the initial analysis. The details were as follows; we chose a SNP closest to 0 cM and the neighboring four SNPs. If the genetic distance of a SNP was the same as that of the next SNP, we considered the genomic position to determine their order. We repeated this process at 1 cM, 2 cM and so on.

We performed a multipoint linkage analysis of the data set (17 613 SNPs) using MERLIN[6] 1.1.2 under the autosomal dominant mode with the following parameters: 0.0001 for disease allele frequency, 1.00 for individuals heterozygous and homozygous for the disease allele and 0.00 for individuals

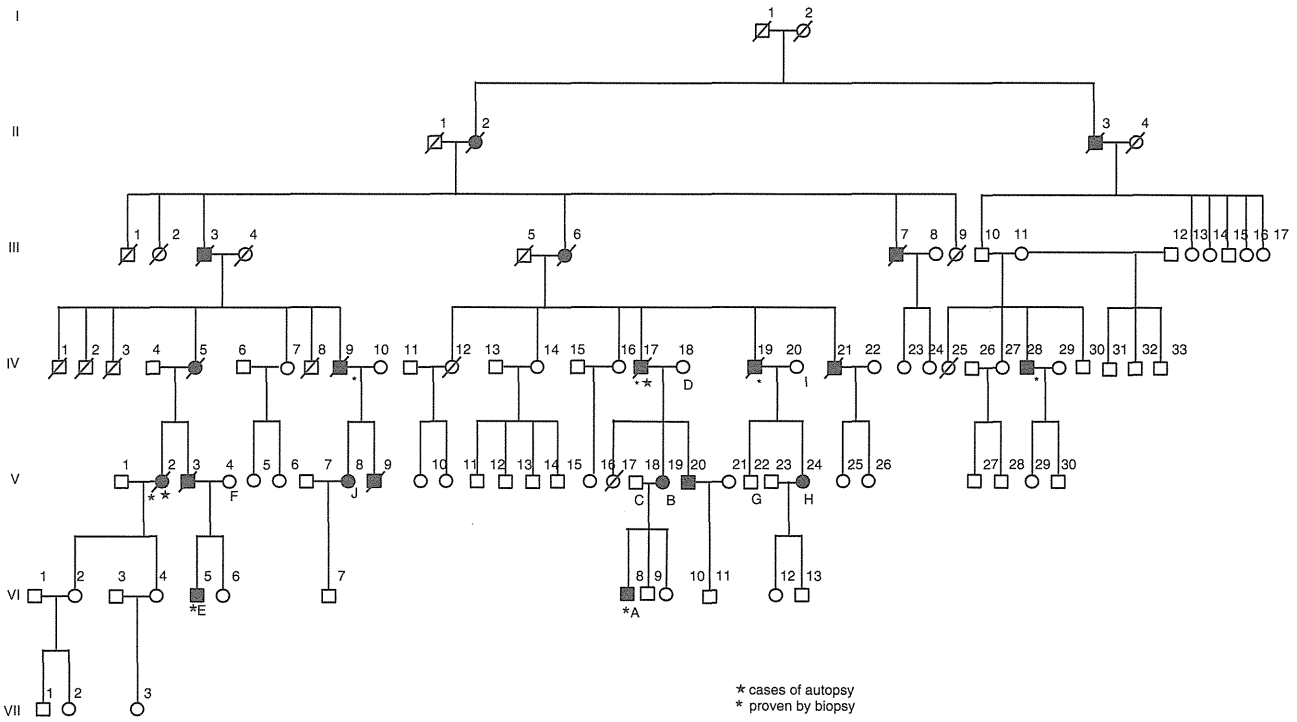

Figure 1 Family pedigree. Filled-in symbols indicate individuals with MFM. Empty symbols indicate unaffected individuals. A star and asterisk indicate autopsy-proven and muscle biopsy-proven cases, respectively. (A–J) indicates individuals whose DNA was used for this study.

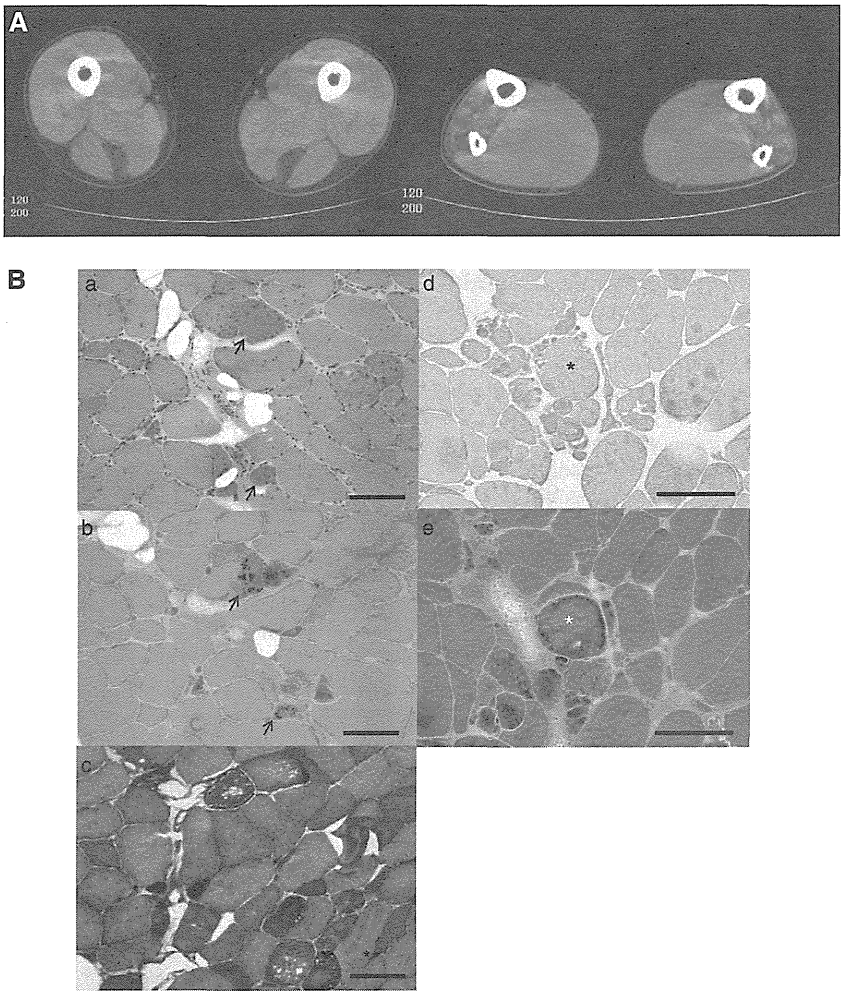

Figure 2 Family clinical data. (**A**) Muscle computed tomography of affected lower extremity. The imaging in the initial assessment of individual A showed symmetrical atrophy and fatty replacement of the semitendinosus in the proximal lower extremities (left) and the tibialis anterior, tibialis posterior, extensor hallucis and digitorum longus, and peroneal muscle in the distal (right) lower extremities. (**B**) Pathology of muscle biopsy. Hematoxylin-eosin (a), Gomori-trichrome (b) and NADH (nicotinamide adenine dinucleotide)-tetrazolium reductase (c) staining of the muscle biopsy sample from the tibialis anterior of individual E are shown. CBs are indicated by arrows. CBs were round or oval, 5–10 μm in diameter and predominantly located in the periphery of type 1 fibers, which stained eosinophilic with hematoxylin-eosin and blue–purple with Gomori-trichrome. NADH-tetrazolium reductase staining showed disorganization of the myofibrillar network. Immunostaining for desmin (d) and Gomori-trichrome staining (e) are serial sections of the muscle biopsy from individual E. Stars indicate corresponding fibers. No strong immunoreaction of desmin was seen in the CBs. Scale bars = 100 μm

homozygous for the alternative allele. After this first analysis, a second analysis was performed with all SNPs fulfilling the above criteria around the peaks identified in the first analysis.

Exome sequencing

Exome sequencing was performed on seven family members in three generations (A–E, H and I in Figure 1), four of whom were affected. Exon capture was performed with the SureSelect Human All Exon kit v2 (individuals E, H and I) or v4 (A–D) (Agilent Technologies, Santa Clara, CA, USA). Exon libraries were sequenced with the Illumina Hiseq 2000 platform according to the manufacturer's instructions (Illumina). Paired 101-base pair reads were aligned to the reference human genome (UCSChg19) using the Burrows-Wheeler Alignment tool.[7] Likely PCR duplicates were removed with the Picard program (http://picard.sourceforge.net/). Single-nucleotide variants and indels were identified using the Genome Analysis Tool Kit (GATK) v1.5 software.[8] SNVs and indels were annotated against the RefSeq database and dbSNP135 with the ANNOVAR program.[9] We used the PolyPhen2 polymorphism phenotyping software tool[10] to predict the functional effects of mutations.

Sanger sequencing

To confirm that mutations identified by exome sequencing segregated with the disease, we performed direct sequencing. PCR was performed with the primers shown in Supplementary Table 1. PCR products were purified with a MultiScreen PCR plate (Millipore, Billerica, MA, USA) and sequenced using BigDye terminator v1.1 and a 3500xL genetic analyzer (Applied Biosystems, Carlsbad, CA, USA).

RESULTS

Linkage analysis

The first linkage analysis identified five regions across autosomes with a logarithm of odds (LOD) score greater than 2 (Figure 3). Of the five regions, two were on chromosome 2 (from 167 cM to 168 cM, with a maximum LOD score of 2.46 and from 182 cM to 185 cM, with a maximum LOD score of 2.71), the other two were on chromosome 8 (from 27 cM to 34 cM, with a maximum LOD score of 2.71 and at 61 cM, with a maximum LOD score of 2.03), and one was on

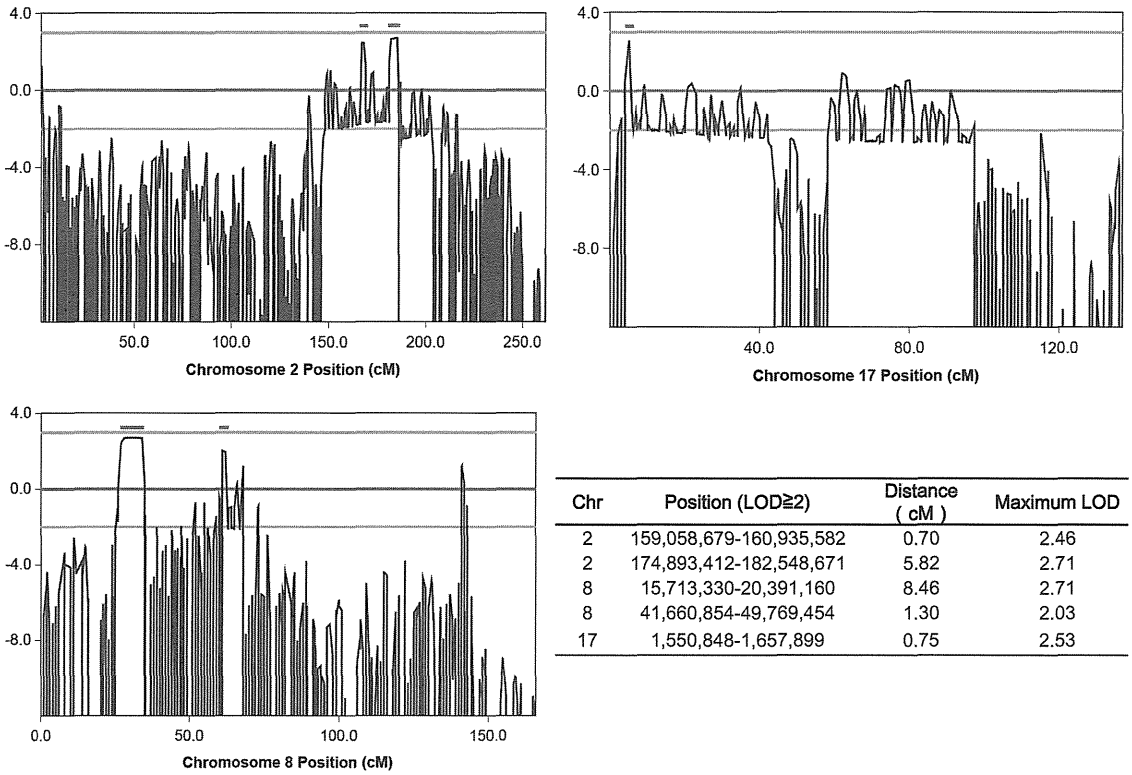

Chr	Position (LOD≧2)	Distance (cM)	Maximum LOD
2	159,058,679-160,935,582	0.70	2.46
2	174,893,412-182,548,671	5.82	2.71
8	15,713,330-20,391,160	8.46	2.71
8	41,660,854-49,769,454	1.30	2.03
17	1,550,848-1,657,899	0.75	2.53

Figure 3 Linkage analysis. Linkage analysis was performed on nine family members (four of them were affected, the others were unaffected) using an Illumina Human Omni 2.5 BeadChip. Five regions with an LOD score greater than 2 (indicated by bar) were identified. A full color version of this figure is available at the *Journal of Human Genetics* journal online.

Table 1 Summary of detected variants by exome sequencing

Individual *Morbidity*	*A* *Affected*	*B* *Affected*	*C* *Unaffected*	*D* *Unaffected*	*E* *Affected*	*H* *Affected*	*I* *Unaffected*	*Segregated in seven family members*
Exonic, splicing	10089	10064	10079	10065	10230	10194	10216	64
Nonsynonymous, splicing, indel, nonsense	4987	5020	5055	5038	5143	5234	5200	32
Allele frequency not available	577	600	536	555	671	794	786	2

chromosome 17 (at 5 cM, with a maximum LOD score of 2.53). In the second detailed linkage analysis, these peaks were determined to range from 167.49 cM at rs4233674 at position 159 058 679 to 168.19 cM at rs7598162 at position 160 935 582, and from 181.23 cM at rs4402725 at position 174 893 412 to 187.05 cM at rs7420169 at position 182 548 671 on chromosome 2; from 26.42 cM at rs2736043 at position 15 713 330 to 34.88 cM at rs9325871 at position 20 391 160, and from 61.02 cM at rs6999814 at position 41 660 854 to 62.32 cM at rs10957281 at position 49 769 454 on chromosome 8; and from 4.7 cM at rs11078552 at position 1 550 848 to 5.45 cM at rs1057355 at position 1 657 899 on chromosome 17. Haplotypes shared by affected individuals in these regions were confirmed by visual inspection. There were a few incompatible SNPs in these regions, presumably due to genotyping error.

Exome sequencing and segregation analysis

In exome sequencing, an average of 215 million reads enriched by SureSelect v4 (SSv4) and 319 million reads enriched by SureSelect v2 (SSv2) were generated, and 99% of reads were mapped to the reference genome by Burrows-Wheeler Alignment tool. An average of 57% (SSv4) and 61% (SSv2) of those reads were duplicated and removed, and an average of 80% (SSv4) and 66% (SSv2) of mapped reads without duplicates were in target regions. The average coverage of each exome was 163-fold (SSv4) and 130-fold (SSv2). An average of 85% (SSv4) and 69% (SSv2) of target regions were covered at least 50-fold (Supplementary Table 2). On average, 10 133 SNVs or indels, which are located within coding exons or splice sites, were identified per individual (Table 1). A total of 64 variants were common among patients and not present in unaffected individuals, and 32 of those were left after excluding synonymous SNVs. In these variants, only the heterozygous mutation c.90263G>T (NM_001256850) at position 179 410 777 of chromosome 2, which was predicted to p.W30088L in *TTN*, was novel (that is, not present in dbSNP v135 or 1000 genomes). Polyphen2 predicted this mutation as probably damaging. This mutation was located in a candidate region suggested by the linkage analysis in the present study. The other variants were registered with dbSNP135, and the allele frequencies, except for one SNV, rs138183879, in *IKBKB*, ranged from 0.0023 to 0.62.

a

Gene	Chr	Position	Variant type	Reference	Variant	dbSNP v135	Coding change	Prediction	Segregaion analysis
TTN	2	179 410777	Missense	G	T	Not present	W30088L	Probably damaging	Segregating
IKBKB	8	42 188 457	Missense	C	T	rs138183879	T742M	Benign	Non-segregating

b

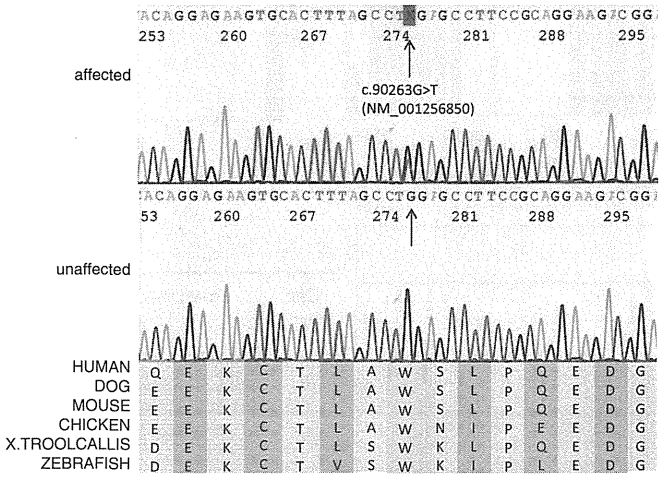

Figure 4 Identified mutations by exome sequencing. (**a**) We performed segregation analysis of two candidates. (**b**) The identified *TTN* mutation and its conservation among species. Sanger sequencing confirmed the heterozygous G to T substitution (indicated by the arrow) at the position chr2;179 410 777, which corresponds to c.90263G>T in exon 293 (NM_001256850.1). The substitution leads to p.W30088L (NP_001243779.1), and this amino acid is conserved among species.

These values were not compatible with the assumption that MFM was a rare disease and showed complete penetrance in this family. The allele frequency of rs138183879 was not available in dbSNP135, and this SNV was in the candidate region on chromosome 8 based on linkage analysis.

We then performed a segregation analysis on the two candidates, the novel mutation c.90263G>T in *TTN* and rs138183879 in *IKBKB*, through Sanger sequencing in 10 family members (A–J in Figure 1; Figure 4a). The rs138183879 SNP was not found in individual J, that is, it was not segregated with the disease in this family. In contrast, the novel mutation c.90263G>T in *TTN* was detected in all patients ($n=5$) and not detected in any of the unaffected family members ($n=5$) or 191 ethnically matched control subjects (382 chromosomes). These results suggested that this rare mutation in *TTN* segregated with the disease in this family.

DISCUSSION

In this study, we found that a novel missense mutation in *TTN* segregated with MFM in a large Japanese family. The identified c.90263G>T mutation in *TTN* (NM_001256850) was considered to be the genetic cause of MFM in our family, because (1) exome sequencing revealed that this was the best candidate mutation after filtering SNPs and indels, (2) this mutation is located in a region on chromosome 2 shared by affected family members, (3) the segregation with MFM was confirmed by Sanger sequencing, (4) this mutation was not detected in 191 control individuals, (5) this mutation was predicted to alter highly conserved amino acids (Figure 4b) and (6) *TTN* encodes a Z-disc-binding molecule called titin, which is similar to all of the previously identified causative genes for MFMs, which also encode Z-disc-associated molecules.

Recently, three mutations in *TTN* have been reported as the causes of hereditary myopathy with early respiratory failure (HMERF, MIM #603689),[11–16] which has similar muscle pathology to MFMs. The identified novel missense mutation c.90263G>T in our study was located on the same exon as recently reported HMERF mutations: c.90272C>T in a Portuguese family[16] and c.90315T>C in Swedish and English families[14,15] (Table 2). This finding suggests the possibility that our family can be recognized as having HMERF from a clinical aspect.

Compared with symptoms described in the past three reports on HMERF (also see Table 2), our patients have common features, such as autosomal dominant inheritance, early respiratory failure, the absence of clinically apparent cardiomyopathy, normal to mild elevation of serum CK and histological findings compatible with MFM. Early involvement of the tibialis anterior is also common, except for the Portuguese family, who reported isolated respiratory insufficiency and a milder presentation of HMERF. Thus, our family shares major clinical manifestations with patients with HMERF, suggesting that the identified mutation is novel for MFM and HMERF.

To date, mutations in *TTN* have been identified in skeletal myopathy and cardiomyopathy.[17,18] The relationship between the variant positions on *TTN* and phenotypes accompanied by skeletal or respiratory muscle involvement is summarized in Table 2. Titin is a large protein (4.20 MDa) that extends from the Z-disk to the M-line within the sarcomere, and it is composed of four major domains: Z-disc, I-band, A-band and M-line (Figure 5). All four HMERF mutations detected by other groups and our study were consistently located in the A-band domain, while mutations in tibial muscular dystrophy (TMD) (MIM #600334),[19–24] limb-girdle muscular dystrophy type 2J (LGMD2J) (#608807)[19,25] and early-onset myopathy with fatal cardiomyopathy (#611705)[26] were located in the M-line domain. HMERF and TMD have some common clinical characteristics, such as autosomal dominant inheritance with onset in adulthood and strong involvement of the tibialis anterior muscle.

Table 2 Previously reported TTN mutations with skeletal and/or respiratory muscle involvement

Phenotype	*LGMD*	*HMERF*	*Our family*	*HMERF*	*HMERF*	*TMD*	*TMD*	*LGMD2J*	*TMD*	*TMD*	*TMD*	*TMD*	*TMD*	*Early-onset myopathy with fatal cardiomyopathy*	*Early-onset myopathy with fatal cardiomyopathy*
Reported by	Vasli *et al.*[16]	Ohlsson *et al.*,[14] Pfeffer *et al.*[15]	Abe *et al.*[5]	Vasli *et al.*[16]	Edstrom *et al.*,[12] Nicolao, *et al.*[11] Lang e *et al.*[13]	Hackman *et al.*[23]	Udd *et al.*,[20] Hackman *et al.*[19]	Udd *et al.*,[25] Hackman *et al.*[19]	Pollazzon *et al.*[24]	Van den Bergh *et al.*[22]	Seze *et al.*,[21] Hackman *et al.*[19]	Hackman *et al.*[23]	Hackman *et al.*[23]	Carmignac *et al.*[26]	Carmignac *et al.*[26]
Mutation identified in Nucleotide (NM_001256850.1)	2012 c.3100G>A, c.52024G>A	2012 c.90315T>C	2012 c.90263G>T	2012 c.90272C>T	2005 c.97348C>T	2008 c.102724delT	2002 102857_ 102867 del11ins11	2002 102857_ 102867 del11ins11	2010 c.102914A>C	2003 c.102917T>A	2002 c.102944T>C	2008 c.102966delA	2008 c.102967C>T	2007 g.289385del ACCAAGTG	2007 g.291297delA
Protein (NP_001243779.1)	p.V1034M, p.A17342T	p.C30071R	p.W30088L	p.P30091L	p.R32450W				p.H34305P	p.I34306N	p.L34315P		p.Q34323X		
Domain	I-band, A-band	A-band (Fn3)	A-band (Fn3)	A-band (Fn3)	A-band (kinase)	M-line	M-line	M-line	M-line	M-line	M-line	M-line	M-line	M-line	M-line
Population	French	Swedish English	Japanese	Portuguese	Swedish	French	Finnish	Finnish	Italian	Belgian	French	Spanish	French	Sudanese	Moroccan
Inheritance	AR	AD	AD	AD	AD	AD	AD	AR	AD	AD	AD	AD	AD	Consanguineous siblings	Consanguineous siblings
Onset	35	33–71	27–45	46	20–50s	20–30s	35–55	20–30s	50–60s	47	45	40–50s	30s	Neonatal	Infant-early childhood
Skeletal muscles															
Major	Proximal UL and LL	TA, PL, EDL, ST	TA, ST	No	TA, neck flexor, proximals	TA, GA,HAM, pelvic	TA	All proximals	TA	TA	TA	TA	TA, HAM, pelvic	General muscle weakness and hypotonia	Psoas, TA, GA, peroneus
Minor		Neck flexor	Cervical, shoulder girdles, intercostals, proximal limb			QF				EDL, peroneal, TP	GA, femoral, scapular	HAM, GA	GA, distal UL		QF, proximal UL, neck, facial, trunk flexor
Spared			Facial			Proximal UL	Facial, UL, proximals	Facial		UL, proximal LL	Facial	UL	Proximal UL, QF		
Cardiac muscles	ND	No	No	ND	ND	ND	No	No	ND	ND	ND	ND	ND	DCM, onset; in the first decade	DCM, onset; 5–12 years old
Respiratory failure	ND	Yes, within 5–8 years	Yes, within 7 years	Isolated respiratory failure	Yes, as first presentation	ND	ND	ND	ND	ND	ND	ND	ND	ND	ND
Muscle pathologic features	ND	Inclusion bodies (major) and RVs (minor)	Cytoplasmic bodies (major) and RVs (minor)	Cytoplasmic bodies	Cytoplasmic bodies, positive for rhodamine-conjugated phalloidin	Dystrophic pattern without vacuoles	Nonspecific dystrophic change	Nonspecific dystrophic change, loss of calpain-3	Dystrophic pattern with RVs	Nonspecific, RV	Nonspecific	Dystrophic pattern with RVs	Nonspecific	Minicore-like lesions and abundant central nuclei	Minicore-like lesions and abundant central nuclei

Abbreviations: AD, autosomal dominant; AR, autosomal recessive; DCM, dilated cardiomyopathy; EDL, extensor digitorum longus; GA, gastrocnemius; HAM, hamstrings; LL, lower limb; ND, not described; no, no involvement; PL, peroneus longus; QF, quadriceps femoris; RV, rimmed vacuole;
ST, semitendinosus; TA, tibialis anterior; TMD, tibial muscular dystrophy; TP, tibialis posterior; UL, upper limb.